An initial phase of JNK activation inhibits cell death early in the endoplasmic reticulum stress response

Max Brown[a-c*], Natalie Strudwick[a-c*], Monika Suwara[a-d*], Louise K. Sutcliffe[a-c, e], Adina D. Mihai[a-c], Ahmed A. Ali[a-c, f], Jamie N. Watson[a-c], and Martin Schröder[a-c]

a) Durham University, School of Biological and Biomedical Sciences, Durham DH1 3LE, United Kingdom.

b) Biophysical Sciences Institute, Durham University, Durham DH1 3LE, United Kingdom.

c) North East England Stem Cell Institute (NESCI), Life Bioscience Centre, International Centre for Life, Central Parkway, Newcastle Upon Tyne, NE1 4EP, UK.

d) Present address: MAST GROUP Ltd., MAST House, Derby Road, Bootle, Merseyside L20 1EA, United Kingdom.

e) Present address: Congenital Heart Disease Research Team, Institute of Genetic Medicine, University of Newcastle, International Centre for Life, Central Parkway, Newcastle upon Tyne, NE1 3BZ, United Kingdom.

f) Molecular Biology Department, National Research Centre, Dokki 12311, Cairo, Egypt.

* These authors contributed equally to this work.

Address for correspondence: Martin Schröder, Durham University, School of Biological and Biomedical Sciences, Durham DH1 3LE, United Kingdom.

phone: +44 (0) 191-334-1316

FAX: +44 (0) 191-334-9104

email: martin.schroeder@durham.ac.uk

Running Title: JNK signalling in the early UPR

Key words: Apoptosis, endoplasmic reticulum, IRE1, JNK, stress response, unfolded protein response

Abbreviations: ER – endoplasmic reticulum, JC-1 - 5,5',6,6'-tetrachloro-1,1',3,3'-tetraethylbenzimidazolylcarbocyanine iodide, MEF – mouse embryonic fibroblast, qPCR – quantitative PCR, RT – reverse transcriptase, UPR – unfolded protein response

Summary statement

Activation of JNK by endoplasmic reticulum stress kinetically precedes activation of XBP1 by IRE1α. JNK-dependent induction of several inhibitors of apoptosis inhibits apoptosis early in the endoplasmic reticulum stress response.

Abstract

Accumulation of unfolded proteins in the endoplasmic reticulum (ER) activates the unfolded protein response (UPR). In mammalian cells, UPR signals generated by several ER membrane resident proteins, including the bifunctional protein kinase endoribonuclease IRE1α, control cell survival and the decision to execute apoptosis. Processing of *XBP1* mRNA by the RNase domain of IRE1α promotes survival of ER stress, while activation of the mitogen-activated protein kinase JNK by IRE1α late in the ER stress response promotes apoptosis. Here we show that activation of JNK in the ER stress response precedes activation of XBP1. This activation of JNK is dependent on IRE1α and TRAF2 and coincides with JNK-dependent induction of expression of several antiapoptotic genes, including *cIAP1*, *cIAP2*, *XIAP*, and *BIRC6*. ER-stressed *jnk1*$^{-/-}$ *jnk2*$^{-/-}$ mouse embryonic fibroblasts (MEFs) display more pronounced mitochondrial permeability transition and increased caspase 3/7 activity compared to wild type MEFs. Caspase 3/7 activity is also elevated in ER-stressed *ciap1*$^{-/-}$ *ciap*2$^{-/-}$, and *xiap*$^{-/-}$ MEFs. These observations suggest that JNK-dependent transcriptional induction of several inhibitors of apoptosis contributes to inhibiting apoptosis early in the ER stress response.

Introduction

Perturbation of protein folding homeostasis in the endoplasmic reticulum (ER) activates several signal transduction pathways collectively called the unfolded protein response (UPR) (Ron and Walter, 2007; Walter and Ron, 2011). In mammalian cells, the UPR is initiated by several ER membrane resident proteins, including the protein kinase-endoribonuclease (RNase) IRE1α (Tirasophon et al., 1998; Wang et al., 1998), the protein kinase PERK (Harding et al., 1999; Shi et al., 1999; Shi et al., 1998), and several type II transmembrane transcription factors such as ATF6α (Yoshida et al., 2000) and CREB-H (Zhang et al., 2006). All of these signalling molecules activate prosurvival, but also proapoptotic responses to ER stress.

These opposing signalling outputs are exemplified by IRE1α. The RNase activity of IRE1α initiates non-spliceosomal splicing of the mRNA for the transcription factor

XBP1 (Calfon et al., 2002; Lee et al., 2002; Shen et al., 2001; Yoshida et al., 2001), which in turn induces transcription of genes encoding ER-resident molecular chaperones (Lee et al., 2003), components of the ER-associated protein degradation machinery (Oda et al., 2006; Yoshida et al., 2003), and several phospholipid biosynthetic genes (Lee et al., 2003; Lee et al., 2008) to promote cell survival. The IRE1α RNase activity also initiates the decay of several mRNAs encoding proteins targeted to the ER (Gaddam et al., 2013; Han et al., 2009; Hollien et al., 2009; Hollien and Weissman, 2006), which decreases the protein folding load of the stressed ER. Degradation of *DR5* mRNA by IRE1α contributes to establishment of a time window for adaptation to ER stress (Lu et al., 2014). On the other hand, IRE1α promotes apoptosis via both its RNase and protein kinase domains. Cleavage of several miRNAs, including miRNA-17, -34a, -96, and -125b, by the RNase domain of IRE1α stabilises and promotes translation of *TXNIP* and *caspase-2* mRNAs (Lerner et al., 2012; Oslowski et al., 2012; Upton et al., 2012). TXNIP promotes apoptosis through activation of caspase-1 and secretion of interleukin 1β (Lerner et al., 2012). The role of caspase-2 in ER stress-induced apoptosis has recently been questioned (Lu et al., 2014; Sandow et al., 2014). The kinase domain of IRE1α activates the mitogen-activated protein (MAP) kinase JNK through formation of a complex with the E3 ubiquitin ligase TRAF2 and the MAP kinase kinase kinase (MAPKKK) ASK1 (Nishitoh et al., 2002; Urano et al., 2000). Sequestration of TRAF2 by IRE1α may also contribute to activation of caspase-12 in murine cells (Yoneda et al., 2001). Pharmacologic (Chen et al., 2008; Huang et al., 2014; Jung et al., 2014; Jung et al., 2012; Smith and Deshmukh, 2007; Teodoro et al., 2012; Wang et al., 2009; Zhang et al., 2001) and genetic (Arshad et al., 2013; Kang et al., 2012) studies have provided evidence that activation of JNK 12 h or later after induction of ER stress is proapoptotic.

Much less is known about the role of JNK at earlier time points in the ER stress response. In tumour necrosis factor (TNF)-α-treated cells two phases of JNK activation can be distinguished (Lamb et al., 2003; Roulston et al., 1998), an early and transient antiapoptotic and a later phase, that coincides with activation of caspases (Roulston et al., 1998). In the early phase JNK induces expression of JunD and the antiapoptotic ubiquitin ligase cIAP2/BIRC3 (Lamb et al., 2003). Furthermore, phosphorylation of Bad at T201 and subsequent inhibition of interaction of Bad with

Bcl-x_L underlies the antiapoptotic role of JNK in interleukin (IL)-3-dependent hematopoietic cells (Yu et al., 2004), while JNK mediates IL-2-dependent survival of T cells through phosphorylation of MCL1 (Hirata et al., 2013). This functional dichotomy of transient and persistent JNK signalling prompted us to investigate whether an initial phase of JNK activation exists in the ER stress response and to characterise the functional significance of such an initial phase of JNK activation in ER-stressed cells.

Results

ER stress activates JNK before XBP1 splicing reaches maximal levels

To investigate how early JNK is activated in the ER stress response we characterised JNK activation over an 8 h time course by monitoring phosphorylation of JNK in its T-loop on T183 and Y185 by Western blotting with antibodies against phosphorylated and total JNK. In mouse embryonic fibroblasts (MEFs), phosphorylation of JNK in its T-loop increased as early as 10 min after addition of 1 μM thapsigargin (Fig. 1A,C) or 10 μg/ml tunicamycin (Fig. 1D,F). JNK phosphorylation returned to near basal levels 8 h after addition of thapsigargin or tunicamycin to cells. The ability of these two mechanistically different ER stressors to elicit rapid phosphorylation of JNK, which over several hours declines to near basal levels, suggests that this initial phase of JNK activation is caused by ER stress invoked by these two chemicals and not a response to secondary effects of these compounds. To compare the kinetics of JNK activation to the kinetics of the *XBP1* splicing reaction and phosphorylation of the PERK substrate eIF2α we monitored *XBP1* splicing by using reverse transcriptase (RT)-PCR and phosphorylation of eIF2α on S51 by Western blotting. Spliced *XBP1* mRNA differs from unspliced *XBP1* mRNA by lacking a 26 nt intron. Hence, the presence of a shorter RT-PCR product on agarose gels is indicative of activation of the IRE1α RNase activity and processing of *XBP1* mRNA. In thapsigargin-treated MEFs ~45% of *XBP1* mRNA were spliced 20 min after addition of thapsigargin (Fig. 1B,C). *XBP1* splicing reached maximal levels only after several hours of thapsigargin treatment, suggesting that activation of JNK precedes maximal activation of XBP1. Phosphorylation of eIF2α was observed within 10 min after induction of ER stress with 1 μM thapsigargin, which indicates that both eIF2α and JNK are phosphorylated before significant levels of *XBP1* mRNA are spliced (Fig. 1B,C). When ER stress was induced with 10 μg/ml tunicamycin, phosphorylation of JNK and eIF2α also preceded

splicing of *XBP1* (Fig. 1D-F). Furthermore, *XBP1* splicing reached maximal levels only after JNK phosphorylation returned to near basal levels in tunicamycin-treated MEFs. In both thapsigargin- and tunicamycin-treated MEFs phosphorylation of eIF2α declined towards the end of the time course, which is consistent with the transient nature of the translational arrest mediated by eIF2α S51 phosphorylation (Kojima et al., 2003; Novoa et al., 2003).

To investigate whether a similar kinetic relationship between phosphorylation of JNK and eIF2α and *XBP1* splicing exists in other cell types, we repeated these experiments with Hep G2 hepatoma cells, 3T3-F442A adipocytes, and C_2C_{12} myotubes. In Hep G2 cells, JNK phosphorylation increased 30 min after addition of 1 μM thapsigargin to the cells and then declined to near resting levels after ~120 min of thapsigargin exposure (Fig. S1A,C). By contrast, 30 min after addition of thapsigargin only ~7% of *XBP1* mRNA were spliced, and after another 15 min *XBP1* splicing was approximately half maximal (Fig. S1B,C). *XBP1* splicing reached maximal levels only after 6 h of thapsigargin treatment. In 3T3-F442A adipocytes phosphorylation of JNK reached a maximum as early as 10 min after application of 1 μM thapsigargin, then returned to basal levels before increasing again towards the end of the time course (Fig. S1D,F). *XBP1* splicing, however, was not detectable until 45 min after addition of thapsigargin, required 4 h to reach maximal levels, and remained at this level for at least another 4 h (Fig. S1E,F). Thus, activation of JNK also precedes activation of XBP1 in Hep G2 cells and 3T3-F442A adipocytes and also returns to near basal levels of JNK activity after several hours of ER stress. We made the same observations in C_2C_{12} myotubes. In these cells an increase in JNK phosphorylation was detected as early as 10 min after induction of ER stress with 1 μM thapsigargin (Fig. S1G,H,J), while the earliest time point at which an increase in *XBP1* splicing was detected was 20 min (Fig. S1I,J). At the same time, activation of JNK diminished over time in C_2C_{12} myotubes, while the level of *XBP1* splicing remained at maximal levels (Fig. S1H-J). In all three cell lines, phosphorylation of both eIF2α and JNK preceded splicing of *XBP1* (Fig. S1). We conclude that activation of JNK preceding induction of *XBP1* splicing and leading to an initial phase of JNK activity are phenomena that can be observed in several ER-stressed murine and human cell types.

The initial phase of JNK activation in ER-stressed cells requires IRE1α and TRAF2

Several different stresses activate JNK (Kyriakis et al., 1994). To examine if the rapid JNK activation seen upon thapsigargin or tunicamycin treatment is in response to ER stress and thus mediated via IRE1α and TRAF2, we characterised whether this rapid JNK activation is IRE1α- and TRAF2-dependent. Activation of JNK in the first ~60 min after induction of ER stress with 1 μM thapsigargin was decreased in *ire1α*$^{-/-}$ and *traf2*$^{-/-}$ MEFs compared to WT MEFs and did no longer reach statistical significance (Figs 1, 2). In both *ire1α*$^{-/-}$ and *traf2*$^{-/-}$ MEFs JNK activation was delayed and reached maximal levels only towards the end of the 8 h time course (Fig. 2). This delayed activation of JNK may be explained by stresses other than and possibly secondary to ER stress, for example oxidative stress (Mauro et al., 2006). Before the onset of the delayed phosphorylation of JNK in *ire1α*$^{-/-}$ and *traf2*$^{-/-}$ MEFs, phosphorylation of JNK was higher in WT MEFs than in the *ire1α*$^{-/-}$ or *traf2*$^{-/-}$ MEFs (Fig. 2G), suggesting that the early JNK activation in ER-stressed cells requires both IRE1α and TRAF2.

To establish if the initial phase of JNK activation is IRE1α- and TRAF2-dependent in cells other than MEFs we characterised whether small interfering (si)-RNA-mediated knockdown of IRE1α or TRAF2 reduces JNK activation by ER stress. Two *IRE1α* siRNAs (#2 and #3, Table S1) reduced *IRE1α* mRNA levels to ~40% of control eGFP siRNA transfected cells 72 h post-transfection (Fig. S2A) and decreased activation of JNK to 60 ± 17% and 30 ± 9% of eGFP siRNA-transfected cells, respectively (Fig. S2B,C). Likewise, two siRNAs against human or murine TRAF2 blunted the ER stress-dependent JNK activation in Hep G2 cells, 3T3-F442A fibroblasts, and C_2C_{12} myoblasts (Figs S2D-F, S3). Furthermore, a dominant negative mutant of TRAF2, TRAF2Δ1-86 (Hsu et al., 1996; Reinhard et al., 1997), which lacks the RING domain (Fig. S4A) inhibited TNF-α-induced JNK activation (Fig. S4B) and blunted the initial phase of JNK activation upon induction of ER stress with 1 μM thapsigargin in 3T3-F442A preadipocytes (Fig. S4C,D) and C_2C_{12} myoblasts (Fig. S4E,F). Taken together, these data demonstrate that the initial phase of JNK activation upon induction of ER stress is mediated by both IRE1α and TRAF2.

The initial phase of JNK activation in ER-stressed cells inhibits cell death via induction of inhibitors of apoptosis (IAPs)

An initial phase of JNK activation by stresses other than ER stress is viewed as being antiapoptotic (Chen et al., 1996a; Lee et al., 1997; Nishina et al., 1997; Raingeaud et al., 1995; Sluss et al., 1994; Traverse et al., 1994). To characterise whether JNK

activation early in the ER stress response is also antiapoptotic, we studied whether mitochondrial permeability transition (MPT) is more pronounced in JNK-deficient MEFs than WT MEFs, because MPT is often observed in apoptotic cells (Bradham et al., 1998; Fulda et al., 1998; Narita et al., 1998; Scorrano et al., 1999). After exposure of cells to 1 μM thapsigargin or 10 μg/ml tunicamycin for up to 4 h MPT was revealed by staining cells with the fluorescent dye 5,5',6,6'-tetrachloro-1,1',3,3'-tetraethylbenzimidazolylcarbocyanine iodide (JC-1) (Reers et al., 1991; Smiley et al., 1991) (Fig. 3A). MPT inhibits accumulation of JC-1 in mitochondria and blue-shifts its fluorescence emission from a punctuate orange to a green fluorescence (Reers et al., 1991). After induction of ER stress with 1 μM thapsigargin for 45 min or 4 h MPT was observed in a greater percentage of *jnk1*$^{-/-}$ *jnk2*$^{-/-}$ MEFs than WT MEFs (Fig. 3A,B). Similar results were obtained when ER stress was induced with 10 μg/ml tunicamycin for 4 h (Fig. 3A,C). To provide further evidence for increased apoptotic cell death in JNK-deficient cells we measured caspase 3/7-like protease activities early in the ER stress response (Fig. 3D,E). Two ER stressors, thapsigargin and tunicamycin, elicited a more pronounced increase of caspase 3/7-like protease activities in *jnk1*$^{-/-}$ *jnk2*$^{-/-}$ MEFs than in WT MEFs 4 h after induction of ER stress (Fig. 3D,E). These data suggest that JNK signalling early in the ER stress response inhibits apoptosis.

In the early antiapoptotic response to TNF-α JNK is required for expression of the mRNA for the antiapoptotic ubiquitin ligase cIAP2/BIRC3 (Lamb et al., 2003). This motivated us to compare the expression of mRNAs for antiapoptotic genes including *cIAP1*, *cIAP2*, *XIAP*, and *BIRC6* at the onset of activation of JNK with 1 μM thapsigargin in WT and *jnk1*$^{-/-}$ *jnk2*$^{-/-}$ MEFs. Expression of the mRNAs for cIAP1, cIAP2, XIAP, and BIRC6 increased in WT cells in the first 45 min of ER stress. By contrast, *cIAP1*, *cIAP2*, and *BIRC6* mRNA levels decreased in *jnk1*$^{-/-}$ *jnk2*$^{-/-}$ cells (Fig. 4). The increase in *XIAP* mRNA was more pronounced in WT than in *jnk1*$^{-/-}$ *jnk2*$^{-/-}$ MEFs, suggesting that JNK positively regulates expression of *XIAP* mRNA (Fig. 4C). To establish whether mammalian inhibitors of apoptosis (IAPs) delay the onset of apoptosis in the early ER stress response we compared caspase 3/7-like protease activity in WT, *ciap1*$^{-/-}$ *ciap2*$^{-/-}$, and *xiap*$^{-/-}$ MEFs. Both *ciap1*$^{-/-}$ *ciap2*$^{-/-}$ and *xiap*$^{-/-}$ MEFs displayed 4.4 ± 1.2 fold higher caspase 3/7-like protease activities than WT MEFs under unstressed conditions (Fig. 5A), which is consistent with increased

susceptibility of these cells and cells treated with IAP antagonists to undergo apoptosis (Conte et al., 2006; Geserick et al., 2009; Schimmer et al., 2004; Vince et al., 2007; Yang and Du, 2004). ER stress induced for 4 h with thapsigargin or tunicamycin resulted in a greater increase in caspase 3/7-like protease activities in *ciap1*$^{-/-}$ *ciap2*$^{-/-}$ and *xiap*$^{-/-}$ MEFs than in WT MEFs (Fig. 5B,C). Taken together, the decreased transcriptional induction of several IAPs in *jnk1*$^{-/-}$ *jnk2*$^{-/-}$ MEFs, increased MPT and increased caspase 3/7-like protease activities in JNK-deficient MEFs, *ciap1*$^{-/-}$ *ciap2*$^{-/-}$, and *xiap*$^{-/-}$ MEFs suggest that JNK-dependent transcriptional induction of several IAPs inhibits apoptosis early in the ER stress response.

Discussion

We show that JNK is activated early in the mammalian UPR and that this immediate JNK activation is antiapoptotic. Activation of JNK early in the UPR by two mechanistically distinct ER stressors, thapsigargin and tunicamycin (Figs 1, S1), and its dependence on IRE1α and TRAF2 (Figs 2, S2-S4) provides evidence that the early JNK activation is in response to ER stress. Greater activation of caspase 3/7-like protease activities and a more rapid MPT were observed in ER-stressed JNK-deficient MEFs than in WT MEFs (Fig. 3). These data support the view that early JNK activation protects ER-stressed cells from executing apoptosis prematurely and are consistent with the observation that *traf2*$^{-/-}$ MEFs are more susceptible to ER stress than WT MEFs (Mauro et al., 2006). Early JNK activation coincides with induction of several antiapoptotic genes (Figs 1, 4). Maximal expression of these mRNAs was JNK-dependent (Fig. 4). MEFs lacking several IAPs, such as *ciap1*$^{-/-}$ *ciap2*$^{-/-}$ and *xiap*$^{-/-}$ MEFs, displayed greater caspase 3/7-like protease activities than WT MEFs during short periods of ER stress (Fig. 5). These observations support the view that IAPs, whose transcriptional induction is JNK-dependent in the early ER stress response, protect cells against apoptosis early in the ER stress response.

Mostly pharmacologic data support that activation of JNK late in the ER stress response promotes cell death (Arshad et al., 2013; Chen et al., 2008; Huang et al., 2014; Jung et al., 2014; Jung et al., 2012; Kang et al., 2012; Smith and Deshmukh, 2007; Tan et al., 2006; Teodoro et al., 2012; Wang et al., 2009; Zhang et al., 2001). Our work suggests that two functionally distinct phases of JNK signalling exist in the ER stress response - an early prosurvival phase and a late phase that promotes cell death. Biphasic JNK signalling with opposing effects on cell viability exists also in

other stress responses. Transient activation of JNK in response to several other stresses is antiapoptotic (Chen et al., 1996a; Lee et al., 1997; Nishina et al., 1997; Raingeaud et al., 1995; Sluss et al., 1994; Traverse et al., 1994), while persistent JNK activation causes cell death (Chen et al., 1996a; Chen et al., 1996b; Guo et al., 1998; Sanchez-Perez et al., 1998). These opposing functional attributes of transient and persistent JNK activation have also been causally established by using JNK-deficient MEFs reconstituted with 1-*tert*-butyl-3-naphthalen-1-ylmethyl-1*H*-pyrazolo[3,4-*d*]pyrimidin-4-ylemine (1NM-PP1)-sensitised alleles of JNK1 and JNK2 (Ventura et al., 2006). Hence, the antiapoptotic function of the initial phase of JNK activation in the ER stress response is another example for the paradigm that the duration of JNK activation controls cell fate. Identification of *cIAP1*, *XIAP*, and *BIRC6* as genes whose expression required JNK in the early response to ER stress (Fig. 4) has allowed us to extend the repertoire of antiapoptotic JNK targets. These, and possibly other genes, may also contribute to how JNK inhibits cell death in other stress responses.

The existence of an initial antiapoptotic phase of JNK signalling in the ER stress response raises at least two questions: 1) What are the molecular mechanisms that define this initial phase as antiapoptotic? 2) Which mechanisms may restrict antiapoptotic JNK signalling to the early response to ER stress? While future experiments will be necessary to answer these questions, possible explanations may be that the duration of activation affects the subcellular localisation of JNKs, that JNK signalling outputs are controlled by molecular determinants, or that the JNK signalling pathway functionally interacts with other signalling pathways, for example the NF-κB pathway.

Opposing signalling outputs of extracellular signal-regulated kinases (ERKs) in PC12 cells have been explained by different subcellular localisations of ERKs (Marshall, 1995). JNK, however, does not appear to relocalise upon stimulation, either in response to transient or persistent activation (Chen et al., 1996a; Sanchez-Perez et al., 1998). This is also the case for JNK activated early in the ER stress response (Fig. 6). An alternative possibility is that JNK substrates function as molecular determinants of the biological functions of transient and persistent JNK activation, respectively. This is, for example, the case for the ERK substrate c-Fos (Murphy et al., 2002).

In the ER stress response NF-κB activation is transient and displays kinetics in several cell lines that are reminiscent of the initial phase of antiapoptotic JNK signalling reported in this study (Deng et al., 2004; Jiang et al., 2003; Wu et al., 2002; Wu et al., 2004). In TNF-α signalling JNK functionally interacts with the NF-κB pathway. JNK activation in the absence of NF-κB is apoptotic (Deng et al., 2003; Guo et al., 1998; Liu et al., 2004; Tang et al., 2002) or necrotic (Ventura et al., 2004), while NF-κB transduces an antiapoptotic response to TNF-α (Devin et al., 2000; Kelliher et al., 1998). At the transcriptional level NF-κB cooperates with JunD (Rahmani et al., 2001), whose phosphorylation is decreased in *jnk1*$^{-/-}$ *jnk2*$^{-/-}$ MEFs (Ventura et al., 2003). NF-κB induces *cIAP1*, *cIAP2*, and *XIAP* (Stehlik et al., 1998). JunD contributes to the transcriptional induction of *cIAP2* in TNF-α-stimulated cells (Lamb et al., 2003). This collaboration between NF-κB and transcription factors controlled by JNK, such as JunD, may explain the JNK-dependent induction of *cIAP1*, *cIAP2*, *XIAP*, and *BIRC6* (Fig. 4), and potentially other antiapoptotic genes, early in the ER stress response.

Transient activation of NF-κB in the ER stress response may also contribute to control of the duration of antiapoptotic JNK signalling. NF-κB inhibits JNK activation by TNF-α (De Smaele et al., 2001; Papa et al., 2004; Reuther-Madrid et al., 2002; Tang et al., 2002; Tang et al., 2001) through induction of XIAP (Tang et al., 2002; Tang et al., 2001) and GADD45β (De Smaele et al., 2001; Papa et al., 2004). TNF-α also induces the dual specificity phosphatase MKP1/DUSP1 (Guo et al., 1998). In murine keratinocytes *cis*-platin induces persistent JNK activation but induces MKP1 only weakly, while transient JNK activation by *trans*-platin correlated with strong induction of MKP1 (Sanchez-Perez et al., 1998). shRNA-mediated knock-down of MKP1 elevated JNK phosphorylation by tunicamycin in C17.2 neural stem cells, which correlated with increased caspase-3 cleavage and decreased cell viability (Li et al., 2011). These observations suggest that MKP1 is a negative regulator of JNK in ER-stressed cells. However, it remains unresolved if the effects of the MKP1 knock-down on caspase-3 cleavage and cell viability are causally mediated via JNK or other MKP1 substrates, such as the p38 MAP kinases (Boutros et al., 2008). In tunicamycin-, but not DTT-treated cerebellar granule neurons S359 phosphorylation and stabilisation of MKP1 were observed, which correlated with short-term JNK activation in tunicamycin-treated cells and prolonged JNK activation in DTT-treated

cells (Li et al., 2011). While these results suggest that MKP1 may control the duration of JNK activation in ER-stressed cells, they may also be the result of different pharmacokinetics or secondary effects of the two ER stressors, especially as JNK is activated by diverse stresses (Kyriakis et al., 1994). For example, DTT chelates heavy metal ions, including Zn^{2+} ions, with p*K* values of ~10-15 (Cornell and Crivaro, 1972; Gnonlonfoun et al., 1991; Krężel et al., 2001) and thus may affect many metal-dependent proteins. DTT can also alter proton gradients over membranes (Petrov et al., 1992), because of its pK_a of ~9.2 (Whitesides et al., 1977), and may reduce lipoamide and through this affect pyruvate dehydrogenase and ATP generation, because its standard redox potential is more negative than the standard redox potential of lipoamide (Cleland, 1964; Massey, 1960). Hence, additional experimentation is required to characterise the role of MKP1 in the ER stress response.

The duration of JNK activation may also be regulated at the level of the ER stress perceiving protein kinase IRE1α. Activation of JNK by IRE1α requires interaction of TRAF2 with IRE1α (Urano et al., 2000). This interaction has not been observed in cells expressing kinase and RNase-defective K599A-IRE1α (Urano et al., 2000). JNK activation precedes *XBP1* splicing (Figs 1, S1). *XBP1* splicing by mammalian IRE1α is stimulated by phosphorylation of IRE1α (Prischi et al., 2014). Hence, overall phosphorylation of IRE1α seems to be an unlikely explanation for the transiency of JNK activation. It is, however, possible that the specific pattern of phosphorylation of the ~10 phosphorylation sites in IRE1α (Itzhak et al., 2014) controls its affinity towards TRAF2 and the activation of JNK by IRE1α.

In conclusion, we show that an initial phase of JNK activation produces antiapoptotic signals early in the ER stress response. Our work also identifies JNK-dependent expression of several antiapoptotic genes, including *cIAP1*, *cIAP2*, and *XIAP*, as a mechanism through which JNK exerts its antiapoptotic functions early in the ER stress response.

Materials and Methods

Antibodies and reagents. Rabbit anti-phospho-S51-eIF2α (cat. no. 9721S, batches 10-12), rabbit anti-JNK (cat. no. 9252, batch 15) rabbit anti-JNK2 (cat. no. 9258, batch 9), rabbit anti-phospho-JNK (cat. no. 4668, batches 9 and 11) antibodies, and human recombinant TNF-α (cat. no. 8902) were purchased from Cell Signaling Technology Inc. (Danvers, MA, USA). The mouse anti-GAPDH antibody (cat. no.

G8795, batch 092M4820V) was purchased from Sigma-Aldrich (Gillingham, UK), the rabbit anti-eIF2α antibody (cat. no. sc-11386, batch G1309) and the rabbit anti-TRAF2 antibody (cat. no. sc-876, batches G1508 and J2009) from Santa Cruz Biotechnology (Santa Cruz, CA, USA), and the mouse anti-emerin antibody (cat. no. ab49499) from Abcam (Cambridge, UK). siRNAs against TRAF2, IRE1α, and eGFP were obtained from Sigma-Aldrich. siRNA sequences are listed in Table S1. Tunicamycin was purchased from Merck Chemicals (Beeston, UK) and thapsigargin from Sigma-Aldrich (Gillingham, UK).

Plasmids. Plasmids were maintained in *Escherichia coli* XL10-Gold cells (Agilent Technologies, Stockport, UK, cat. no. 200314). Standard protocols for plasmid constructions were used. Plasmid pMT2T-TRAF2Δ1-86 was generated by amplifying a 1,327 bp fragment from pMT2T-HA-TRAF2 (Leonardi et al., 2000) with primers H8215 and H8216 (Table S2). The PCR product was cleaved with *Cla*I and *Not*I and cloned into *Cla*I- and *Not*I-digested pMT2T-HA-TRAF2 to yield pMT2T-TRAF2Δ1-86. The TRAF2 region in pMT2T-TRAF2Δ1-86 was confirmed by sequencing.

Cell culture. WT, *ire1α*$^{-/-}$ (Lee et al., 2002), *jnk1*$^{-/-}$ *jnk2*$^{-/-}$ (Tournier et al., 2000), *traf2*$^{-/-}$ (Yeh et al., 1997), *ciap1*$^{-/-}$ *ciap2*$^{-/-}$ (Geserick et al., 2009), and *xiap*$^{-/-}$ (Vince et al., 2008) MEFs were provided by R. J. Kaufman (Sanford Burnham Medical Research Institute, La Jolla, CA, USA), R. Davis (University of Massachusetts, Worchester, MA, USA), T. Mak (University of Toronto, Ontario Cancer Institute, Toronto, Ontario, Canada), and J. Silke (Walter+Eliza Hall Institute for Medical Research, Victoria, Australia), respectively. 3T3-F442A preadipocytes (Green and Kehinde, 1976), C_2C_{12} myoblasts (Blau et al., 1985), and Hep G2 cells (Knowles et al., 1980) were obtained from C. Hutchison (Durham University), R. Bashir (Durham University), and A. Benham (Durham University), respectively. All cell lines were tested for mycoplasma contamination upon receipt in the laboratory with the EZ-PCR mycoplasma test kit from Geneflow (cat. no. K1-0210, Lichfield, UK). Mycoplasma testing was repeated every ~3 months with all cells in culture at that time. Contaminated cultures were discarded.

All cell lines were grown at 37°C in an atmosphere of 95% (v/v) air, 5% (v/v) CO_2, and 95% humidity. Hep G2 cells were grown in minimal essential medium (MEM) (Eagle, 1959) supplemented with 10% (v/v) foetal bovine serum (FBS) and 2 mM L-glutamine. All other cell lines were grown in Dulbecco's modified Eagle's

medium (DMEM) containing 4.5 g/l D-glucose (Morton, 1970; Rutzky and Pumper, 1974), 10% (v/v) FBS, and 2 mM L-glutamine. The medium for *ire1α*$^{-/-}$ and corresponding WT MEFs was supplemented with 110 mg/l pyruvate (Lee et al., 2002). To differentiate C_2C_{12} cells 60-70% confluent cultures were shifted into low mitogen medium consisting of DMEM containing 4.5 g/l D-glucose, 2% (v/v) horse serum, and 2 mM L-glutamine and incubated for another 7-8 d while replacing the low mitogen medium every 2-3 d (Bains et al., 1984). Differentiation of C_2C_{12} cells was assessed by microscopic inspection of cultures, staining of myotubes with rhodamine-labelled phalloidin (Amato et al., 1983), and reverse transcriptase PCR for transcription of the genes encoding *S*-adenosyl-homocysteine hydrolase (*AHCY*), myosin light chain 1 (*MYL1*), and troponin C (*TNNC1*, Fig. S1G). 3T3-F442A fibroblasts were differentiated into adipocytes as described before (Mihai and Schröder, 2015). Adipocyte differentiation was assessed by analysing nile red-stained cells by flow cytometry as described before (Mihai and Schröder, 2015). ER stress was induced with 1 μM thapsigargin or 10 μg/ml tunicamycin, if not stated otherwise.

Hep G2 cells were transfected with plasmids using jetPRIME (Polyplus Transfection, Illkirch, France, cat. no. 114) and with siRNAs using INTERFERin (Polyplus Transfection, cat. no. 409) transfection reagents. Plasmids and siRNAs were transfected into all other cell lines by electroporation with a Neon electroporator (Life Technologies, Paisley, UK) using a 10 μl tip. Manufacturer-optimised electroporation conditions were used for 3T3-F442A preadipocytes and C_2C_{12} myoblasts. MEFs were electroporated with one pulse of 1200 V and a pulse width of 30 ms. 10-20 nM of each siRNA were transfected. The control siRNA was designed against the enhanced green fluorescent protein (eGFP) from *Aequora victoria*. Transfection efficiencies were determined by transfection of 2 μg of pmaxGFP (Lonza Cologne GmbH, Cologne, Germany) and detection of GFP-expressing cells with a Zeiss ApoTome fluorescence microscope. Transfection efficiencies were >80%. 24 h after transfection cells were analysed or time courses initiated, if not stated otherwise.

RNA extraction and RT-PCRs. RNA was extracted with the EZ-RNA total RNA isolation kit (Geneflow, cat. no. K1-0120) and reverse transcribed with oligo-dT primers (Promega, Southampton, cat. no. C1101) and Superscript III reverse transcriptase (Life Technologies, cat. no. 18080044) as described previously (Cox et al., 2011). Protocols for detection of splicing of murine and human *XBP1* have been

described previously (Cox et al., 2011). In brief, 2.5 µl of the cDNA synthesis reaction were amplified with 1 µM of primers H8289 and H8290 for human *XBP1* and primers H7961 and H7962 for murine *XBP1* in a 50 µl reaction containing 1 x GoTaq reaction buffer (Promega, cat. no. M7911), 1.5 mM $MgCl_2$, 200 µM dNTPs, and 0.05 U/ml GoTaq hot start polymerase (Promega, cat. no. M5001). The reaction was incubated for 2 min at 94°C, and then cycled for 35 cycles consisting of subsequent incubations at 94°C for 1 min, 59°C for 1 min, and 72°C for 30 s, followed by a final extension step at 72°C for 5 min. *ACTB* was amplified under the same conditions as described for *XBP1* except that GoTaq G2 Flexi DNA polymerase (Promega, cat. no. M7801) was used. Human *ACTA1* was amplified with primers H8287 and H8288 and murine *ACTB* with primers H7994 and H7995. Primer sequences are listed in Table S2. Band intensities were quantified using ImageJ (Collins, 2007) and the percentage of *XBP1* splicing calculated by dividing the signal for spliced *XBP1* mRNA by the sums of the signals for spliced and unspliced *XBP1* mRNAs. Quantitative PCRs (qPCRs) were run on a Rotorgene 3000 (Qiagen, Crawley, UK). Amplicons were amplified with 0.5 µl 5 U/µl GoTaq® Flexi DNA polymerase (Promega, cat. no. M8305), 2 mM $MgCl_2$, 200 µM dNTPs, and 1 µM of each primer and detected with a 1:167,000 fold dilution of a SybrGreen stock solution (Life Technologies, cat. no. S7563) or the GoTaq qPCR Master Mix from Promega (cat. no. A6002). Primers for qPCR are listed in Table S2. qPCR using GoTaq DNA polymerase were performed as follows. After denaturation for 2 min at 95°C samples underwent 40 cycles of denaturation at 95°C for 30 s, primer annealing at 58°C for 30 s, and primer extension at 72°C for 30 s. After denaturation at 95°C for 2 min qPCRs with the GoTaq qPCR Master mix were cycled 40 times at 95°C for 15 s, 60°C for 15 s, and 72°C for 15 s for *cIAP1*, *cIAP2*, *XIAP*, and *BRUCE* and 40 times at 95°C for 15 s, 60°C for 60 s for *ACTB*. Fluorescence data were acquired during the annealing step or in case of qPCR amplification of *ACTB* with the GoTaq qPCR Master Mix during the first 30 s at 60°C. Amplification of a single PCR product was confirmed by recording the melting curves after each PCR run. Average amplification efficiencies in the exponential phase were calculated using the comparative quantification analysis in the Rotor Gene Q software and were between 0.6 and 0.7 for all qPCRs. C_T values were calculated and normalised to *GAPDH*, *ACTA1*, or *ACTB* mRNA levels as described by Pfaffl (Pfaffl, 2001) taking the average amplification efficiencies into

account. Results represent the average and standard error (s.e.m.) of three technical repeats. qPCR results were confirmed by at least one other biological replicate. Murine *AHCY*, *MYL1*, and *TNNC* qPCRs were standardised to *GAPDH*, murine *BIRC6*, *cIAP1*, *cIAP2*, *TRAF*2, and *XIAP* qPCRs to *ACTB*, the human *IRE1*α qPCR to GAPDH and the human *TRAF2* qPCR to *ACTA1*.

Cell lysis and Western blotting. Cells were washed three times with ice-cold phosphate-buffered saline (PBS, 4.3 mM Na_2HPO_4, 1.47 mM KH_2PO_4, 27 mM KCl, 137 mM NaCl, pH 7.4) and lysed in RIPA buffer [50 mM Tris-HCl, pH 8.0, 150 mM NaCl, 0.5% (w/v) sodium deoxycholate, 0.1% (v/v) Triton X-100, 0.1% (w/v) SDS] containing Roche complete protease inhibitors (Roche Applied Science, Burgess Hill, UK, cat. no. 11836153001) as described before (Cox et al., 2011).

For isolation of cytosolic and nuclear fractions cells were washed two times with ice-cold PBS and gently lysed in 0.32 M sucrose, 10 mM Tris-HCl pH 8.0, 3 mM $CaCl_2$, 2 mM $Mg(OAc)_2$, 0.1 mM EDTA, 0.5% (v/v) NP-40, 1 mM DTT, 0.5 mM PMSF. Nuclei were collected by centrifugation for 5 min at 2,400 g, 4°C. The supernatant was used as the cytosolic fraction. The nuclear pellet was resuspended in 0.32 M sucrose, 10 mM Tris HCl pH 8.0, 3 mM $CaCl_2$, 2 mM $Mg(OAc)_2$, 0.1 mM EDTA, 1 mM DTT, 0.5 mM PMSF by flipping the microcentrifuge tube. The nuclei were collected by centrifugation for 5 min at 2,400 g, 4°C. After aspiration of all of the wash buffer the nuclei were resuspended in 30 µl low salt buffer [20 mM HEPES (pH 7.9), 1.5 mM $MgCl_2$, 20 mM KCl, 0.2 mM EDTA, 25% (v/v) glycerol, 0.5 mM DTT, 0.5 mM PMSF] by flipping the microcentrifuge tube. One volume of high salt buffer [20 mM HEPES (pH 7.9), 1.5 mM $MgCl_2$, 800 mM KCl, 0.2 mM EDTA, 25% glycerol (v/v), 1% NP-40, 0.5 mM DTT, 0.5 mM PMSF] was added drop wise while continuously mixing the contents of the microcentrifuge tube by flipping. The tubes were then incubated for 45 min at 4°C on an end-over-end rotator. The tubes were centrifuged at 14,000 g for 15 min at 4°C and the supernatant transferred into a fresh microcentrifuge tube to obtain the nuclear extract.

Proteins were separated by SDS-PAGE and transferred to polyvinylidene difluoride (PVDF) membranes (Amersham HyBond^{TM}-P, pore size 0.45 µm, GE Healthcare, Little Chalfont, UK, cat. no. RPN303F) by semi-dry electrotransfer in 0.1 M Tris, 0.192 M glycine, and 5% (v/v) methanol at 2 mA/cm^2 for 60-75 min. Membranes were blocked for 1 h in 5% (w/v) skimmed milk powder in TBST [20

mM Tris-HCl, pH 7.6, 137 mM NaCl, and 0.1% (v/v) Tween-20] or 5% bovine serum albumin (BSA) in TBST and then incubated overnight with the primary antibody at 4°C and gentle agitation. Blots were washed three times with TBST and then probed with secondary antibody for 1 h at room temperature. The anti-eIF2α, anti-phospho-S51-eIF2α, anti-JNK, anti-phospho-JNK, and anti-TRAF2 antibodies were used at a 1:1,000 dilution in TBST + 5% (w/v) BSA. Membranes were then developed with goat anti-rabbit-IgG (H+L)-horseradish peroxidase (HRP)-conjugated secondary antibody (Cell Signaling, cat. no. 7074S, batch 24) at a 1:1,000 dilution in TBST + 5% (w/v) skimmed milk powder. The mouse anti-GAPDH antibody was used at a 1:30,000 dilution in TBST + 5% (w/v) skimmed milk powder and developed with goat anti-mouse IgG (H+L)-HRP-conjugated secondary antibody (Thermo Scientific, cat. no. 31432, batch OE17149612) at a 1:20,000 dilution in TBST + 5% (w/v) skimmed milk powder. For signal detection Pierce ECL Western Blotting Substrate (cat. no. 32209) or Pierce ECL 2 Western Blotting Substrate (cat. no. 32132) from Thermo Fisher Scientific (Loughborough, UK) were used. Blots were exposed to CL-X Posure™ film (Thermo Fisher Scientific, Loughborough, UK, cat. no. 34091). Exposure times were adjusted on the basis of previous exposures to obtain exposures in the linear range of the film. Films were scanned on a CanoScan LiDE 600F scanner (Canon) and saved as tif files. Bands were quantified using ImageJ exactly as described under the heading “Gels Submenu” on the ImageJ web site (http://rsb.info.nih.gov/ij/docs/menus/analyze.html#plot). In case of unphosphorylated proteins intensities for the experimental antibody were divided by the intensities obtained with the antibody for the loading control in the same lane to correct for differences in loading between lanes. Intensities for phosphorylated eIF2α were divided by the intensities obtained for total eIF2α in the same lane. For phosphorylated and total JNK, the sums of the intensities at 54 kDa and 46 kDa, which both represent several JNK1 and JNK2 isoforms (Gupta et al., 1996), were used to calculate the fraction of phosphorylated JNK in a similar way as described for phospho-eIF2α. Normalisation of phospho-JNK signals to JNK2 or GAPDH gave qualitatively the same results. All loading control- or unphosphorylated protein-corrected intensities obtained for one Western blot were then expressed relative to the loading control-corrected intensity of the 0 h sample in this Western blot. To reprobe blots for detection of nonphosphorylated proteins, membranes were stripped using

Restore Western Blot Stripping Buffer (Thermo Fisher Scientific, cat. no. 21059) and blocked with 5% (w/v) skimmed milk powder in TBST.

Caspase 3 and 7-like activities were determined with the Caspase-Glo 3/7 kit from Promega (cat. no. G8091). Luminescence was read with a Synergy H4 Multi-Mode Microplate Reader (BioTek, Swindon, UK) and standardised to total protein concentrations determined with the *DC* protein assay from Bio-Rad Laboratories (Hemel Hempstead, UK, cat. no. 500-0116).

Fluorescence microscopy. For confocal microscopy cells were grown in lumox dishes (Sarstedt, Leichester, UK, cat. no. 94.6077.331). After incubation with 1 μM thapsigargin cells were incubated with 2 μg/ml JC-1 (Life Technologies, cat. no. T3168) at 37°C for 20 min (Ankarcrona et al., 1995; Cossarizza et al., 1993; Reers et al., 1991; Smiley et al., 1991). The cells were washed twice with PBS before addition of fresh medium for live cell imaging on a Leica TCS SP5 II confocal microscope (Leica Microsystems, Mannheim, Germany). JC-1 fluorescence was excited at 488 nm with an argon laser set at 22% of its maximum power. Green fluorescence between 515-545 nm was collected with a photomultiplier tube and orange fluorescence between 590-620 nm with a HyD 5 detector. Cells showing fluorescence emission between 515-545 nm only were counted as having undergone MPT, while cells that displayed punctuate fluorescence emission between 590-620 nm were counted as not having undergone MPT.

Error and statistical calculations. Samples sizes (*n*) were derived from experiments with independent cell cultures. Experimental data are presented as the mean and its s.e.m. For composite parameters, errors were propagated using the law of error propagation for random, independent errors (Ku, 1966). Statistical calculations were performed in GraphPad Prism 6.07 (GraphPad Software, La Jolla, CA, USA).

Acknowledgements

This work was supported by the European Community's 7th Framework Programme (FP7/2007-2013) under grant agreement no. 201608, a PhD studentship grant to support A.D.M from Diabetes UK (BDA 09/0003949), and a PhD studentship grant to support M.B. from Parkinson's UK (H-1004). We thank A. Benham (Durham University), R. Bashir (Durham University), R. Davis (University of Massachusetts), C. Hutchison (Durham University), R. J. Kaufman (Sanford Burnham Medical Research Institute), T. Mak (University of Toronto), and J. Silke (Walter+Eliza Hall

Institute for Medical Research) for providing cell lines. We thank U. Siebenlist (NIAID, NIH) for providing plasmid pMT2T-HA-TRAF2.

Author contributions

M.Sc. conceived the project, M.B., N.S., and M.Sc. designed the experiments, M.B,, N.S., M.Su, L.K.S., A.D.M., A.A.A., and J.N.W. performed experiments, and M.Sc., M.B., and N.S. analysed and interpreted the data. M.Sc. wrote the manuscript. All authors reviewed and approved the manuscript.

References

Amato, P. A., Unanue, E. R. and Taylor, D. L. (1983). Distribution of actin in spreading macrophages: a comparative study on living and fixed cells. *J Cell Biol* **96**, 750-61.

Ankarcrona, M., Dypbukt, J. M., Bonfoco, E., Zhivotovsky, B., Orrenius, S., Lipton, S. A. and Nicotera, P. (1995). Glutamate-induced neuronal death: a succession of necrosis or apoptosis depending on mitochondrial function. *Neuron* **15**, 961-73.

Arshad, M., Ye, Z., Gu, X., Wong, C. K., Liu, Y., Li, D., Zhou, L., Zhang, Y., Bay, W. P., Yu, V. C. et al. (2013). RNF13, a RING finger protein, mediates endoplasmic reticulum stress-induced apoptosis through the IRE1alpha/JNK pathway. *J Biol Chem* **288**, 8726-36.

Bains, W., Ponte, P., Blau, H. and Kedes, L. (1984). Cardiac actin is the major actin gene product in skeletal muscle cell differentiation in vitro. *Mol Cell Biol* **4**, 1449-53.

Blau, H. M., Pavlath, G. K., Hardeman, E. C., Chiu, C. P., Silberstein, L., Webster, S. G., Miller, S. C. and Webster, C. (1985). Plasticity of the differentiated state. *Science* **230**, 758-66.

Boutros, T., Nantel, A., Emadali, A., Tzimas, G., Conzen, S., Chevet, E. and Metrakos, P. P. (2008). The MAP kinase phosphatase-1 MKP-1/DUSP1 is a regulator of human liver response to transplantation. *Am J Transplant* **8**, 2558-68.

Bradham, C. A., Qian, T., Streetz, K., Trautwein, C., Brenner, D. A. and Lemasters, J. J. (1998). The mitochondrial permeability transition is required for tumor necrosis factor alpha-mediated apoptosis and cytochrome *c* release. *Mol Cell Biol* **18**, 6353-64.

Calfon, M., Zeng, H., Urano, F., Till, J. H., Hubbard, S. R., Harding, H. P., Clark, S. G. and Ron, D. (2002). IRE1 couples endoplasmic reticulum load to secretory capacity by processing the *XBP-1* mRNA. *Nature* **415**, 92-6.

Chen, C.-L., Lin, C.-F., Chang, W.-T., Huang, W.-C., Teng, C.-F. and Lin, Y.-S. (2008). Ceramide induces p38 MAPK and JNK activation through a mechanism involving a thioredoxin-interacting protein-mediated pathway. *Blood* **111**, 4365-74.

Chen, Y.-R., Meyer, C. F. and Tan, T.-H. (1996a). Persistent activation of c-Jun N-terminal kinase 1 (JNK1) in γ radiation-induced apoptosis. *J Biol Chem* **271**, 631-4.

Chen, Y. R., Wang, X., Templeton, D., Davis, R. J. and Tan, T. H. (1996b). The role of c-Jun N-terminal kinase (JNK) in apoptosis induced by ultraviolet C and gamma radiation. Duration of JNK activation may determine cell death and proliferation. *J Biol Chem* **271**, 31929-36.

Cleland, W. W. (1964). Dithiothreitol, a new protective reagent for SH groups. *Biochemistry* **3**, 480-2.

Collins, T. J. (2007). ImageJ for microscopy. *BioTechniques* **43**, 25-30.

Conte, D., Holcik, M., Lefebvre, C. A., Lacasse, E., Picketts, D. J., Wright, K. E. and Korneluk, R. G. (2006). Inhibitor of apoptosis protein cIAP2 is essential for lipopolysaccharide-induced macrophage survival. *Mol Cell Biol* **26**, 699-708.

Cornell, N. W. and Crivaro, K. E. (1972). Stability constant for the zinc-dithiothreitol complex. *Anal Biochem* **47**, 203-8.

Cossarizza, A., Baccarani-Contri, M., Kalashnikova, G. and Franceschi, C. (1993). A new method for the cytofluorimetric analysis of mitochondrial membrane potential using the J-aggregate forming lipophilic cation 5,5',6,6'-tetrachloro-1,1',3,3'-tetraethylbenzimidazolcarbocyanine iodide (JC-1). *Biochem Biophys Res Commun* **197**, 40-5.

Cox, D. J., Strudwick, N., Ali, A. A., Paton, A. W., Paton, J. C. and Schröder, M. (2011). Measuring signaling by the unfolded protein response. *Methods Enzymol* **491**, 261-92.

De Smaele, E., Zazzeroni, F., Papa, S., Nguyen, D. U., Jin, R., Jones, J., Cong, R. and Franzoso, G. (2001). Induction of *gadd45β* by NF-κB downregulates pro-apoptotic JNK signalling. *Nature* **414**, 308-13.

Deng, J., Lu, P. D., Zhang, Y., Scheuner, D., Kaufman, R. J., Sonenberg, N., Harding, H. P. and Ron, D. (2004). Translational repression mediates activation of

nuclear factor kappa B by phosphorylated translation initiation factor 2. *Mol Cell Biol* **24**, 10161-8.

Deng, Y., Ren, X., Yang, L., Lin, Y. and Wu, X. (2003). A JNK-dependent pathway is required for TNFα-induced apoptosis. *Cell* **115**, 61-70.

Devin, A., Cook, A., Lin, Y., Rodriguez, Y., Kelliher, M. and Liu, Z.-g. (2000). The distinct roles of TRAF2 and RIP in IKK activation by TNF-R1: TRAF2 recruits IKK to TNF-R1 while RIP mediates IKK activation. *Immunity* **12**, 419-29.

Dunnett, C. W. (1955). A multiple comparison procedure for comparing several treatments with a control. *J Am Stat Assoc* **50**, 1096-121.

Dunnett, C. W. (1964). New tables for multiple comparisons with control. *Biometrics* **20**, 482-91.

Eagle, H. (1959). Amino acid metabolism in mammalian cell cultures. *Science* **130**, 432-7.

Fulda, S., Scaffidi, C., Susin, S. A., Krammer, P. H., Kroemer, G., Peter, M. E. and Debatin, K.-M. (1998). Activation of mitochondria and release of mitochondrial apoptogenic factors by betulinic acid. *J Biol Chem* **273**, 33942-8.

Gaddam, D., Stevens, N. and Hollien, J. (2013). Comparison of mRNA localization and regulation during endoplasmic reticulum stress in *Drosophila* cells. *Mol Biol Cell* **24**, 14-20.

Geserick, P., Hupe, M., Moulin, M., Wong, W. W., Feoktistova, M., Kellert, B., Gollnick, H., Silke, J. and Leverkus, M. (2009). Cellular IAPs inhibit a cryptic CD95-induced cell death by limiting RIP1 kinase recruitment. *J Cell Biol* **187**, 1037-54.

Gnonlonfoun, N., Filella, M. and Berthon, G. (1991). Lead (II)-dithiothreitol equilibria and their potential influence on lead inhibition of 5-aminolevulinic acid dehydratase in in vitro assays. *J Inorg Biochem* **42**, 207-15.

Green, H. and Kehinde, O. (1976). Spontaneous heritable changes leading to increased adipose conversion in 3T3 cells. *Cell* **7**, 105-13.

Guo, Y.-L., Baysal, K., Kang, B., Yang, L.-J. and Williamson, J. R. (1998). Correlation between sustained c-Jun N-terminal protein kinase activation and apoptosis induced by tumor necrosis factor-α in rat mesangial cells. *J Biol Chem* **273**, 4027-34.

Gupta, S., Barrett, T., Whitmarsh, A. J., Cavanagh, J., Sluss, H. K., Dérijard, B. and Davis, R. J. (1996). Selective interaction of JNK protein kinase isoforms with transcription factors. *EMBO J* **15**, 2760-70.

Han, D., Lerner, A. G., Vande Walle, L., Upton, J.-P., Xu, W., Hagen, A., Backes, B. J., Oakes, S. A. and Papa, F. R. (2009). IRE1α kinase activation modes control alternate endoribonuclease outputs to determine divergent cell fates. *Cell* **138**, 562-75.

Harding, H. P., Zhang, Y. and Ron, D. (1999). Protein translation and folding are coupled by an endoplasmic-reticulum-resident kinase. *Nature* **397**, 271-4.

Hirata, Y., Sugie, A., Matsuda, A., Matsuda, S. and Koyasu, S. (2013). TAK1-JNK axis mediates survival signal through Mcl1 stabilization in activated T cells. *J Immunol* **190**, 4621-6.

Hollien, J., Lin, J. H., Li, H., Stevens, N., Walter, P. and Weissman, J. S. (2009). Regulated Ire1-dependent decay of messenger RNAs in mammalian cells. *J Cell Biol* **186**, 323-31.

Hollien, J. and Weissman, J. S. (2006). Decay of endoplasmic reticulum-localized mRNAs during the unfolded protein response. *Science* **313**, 104-7.

Hsu, H., Shu, H. B., Pan, M. G. and Goeddel, D. V. (1996). TRADD-TRAF2 and TRADD-FADD interactions define two distinct TNF receptor 1 signal transduction pathways. *Cell* **84**, 299-308.

Huang, Y., Li, X., Wang, Y., Wang, H., Huang, C. and Li, J. (2014). Endoplasmic reticulum stress-induced hepatic stellate cell apoptosis through calcium-mediated JNK/P38 MAPK and calpain/caspase-12 pathways. *Mol Cell Biochem* **394**, 1-12.

Itzhak, D., Bright, M., McAndrew, P., Mirza, A., Newbatt, Y., Strover, J., Widya, M., Thompson, A., Morgan, G., Collins, I. et al. (2014). Multiple autophosphorylations significantly enhance the endoribonuclease activity of human inositol requiring enzyme 1α. *BMC Biochem* **15**, 3.

Jiang, H. Y., Wek, S. A., McGrath, B. C., Scheuner, D., Kaufman, R. J., Cavener, D. R. and Wek, R. C. (2003). Phosphorylation of the α subunit of eukaryotic initiation factor 2 is required for activation of NF-κB in response to diverse cellular stresses. *Mol Cell Biol* **23**, 5651-63.

Jung, T. W., Hwang, H.-J., Hong, H. C., Choi, H. Y., Yoo, H. J., Baik, S. H. and Choi, K. M. (2014). Resolvin D1 reduces ER stress-induced apoptosis and

triglyceride accumulation through JNK pathway in HepG2 cells. *Mol Cell Endocrinol* **391**, 30-40.

Jung, T. W., Lee, M. W., Lee, Y. J. and Kim, S. M. (2012). Metformin prevents thapsigargin-induced apoptosis via inhibition of c-Jun NH_2 terminal kinase in NIT-1 cells. *Biochem Biophys Res Commun* **417**, 147-52.

Kang, M.-J., Chung, J. and Ryoo, H. D. (2012). CDK5 and MEKK1 mediate pro-apoptotic signalling following endoplasmic reticulum stress in an autosomal dominant retinitis pigmentosa model. *Nat Cell Biol* **14**, 409-15.

Kelliher, M. A., Grimm, S., Ishida, Y., Kuo, F., Stanger, B. Z. and Leder, P. (1998). The death domain kinase RIP mediates the TNF-induced NF-κB signal. *Immunity* **8**, 297-303.

Knowles, B. B., Howe, C. C. and Aden, D. P. (1980). Human hepatocellular carcinoma cell lines secrete the major plasma proteins and hepatitis B surface antigen. *Science* **209**, 497-9.

Kojima, E., Takeuchi, A., Haneda, M., Yagi, A., Hasegawa, T., Yamaki, K.-i., Takeda, K., Akira, S., Shimokata, K. and Isobe, K. (2003). The function of GADD34 is a recovery from a shutoff of protein synthesis induced by ER stress: elucidation by GADD34-deficient mice. *FASEB J* **17**, 1573-5.

Krężel, A., Leśniak, W., Jeżowska-Bojczuk, M., Mlynarz, P., Brasuñ, J., Kozlowski, H. and Bal, W. (2001). Coordination of heavy metals by dithiothreitol, a commonly used thiol group protectant. *J Inorg Biochem* **84**, 77-88.

Ku, H. H. (1966). Notes on use of propagation of error formulas. *J Res Nat Bureau Standards Sect C - Eng Instrumentat* **70**, 263-73.

Kyriakis, J. M., Banerjee, P., Nikolakaki, E., Dai, T., Rubie, E. A., Ahmad, M. F., Avruch, J. and Woodgett, J. R. (1994). The stress-activated protein kinase subfamily of c-Jun kinases. *Nature* **369**, 156-60.

Lamb, J. A., Ventura, J. J., Hess, P., Flavell, R. A. and Davis, R. J. (2003). JunD mediates survival signaling by the JNK signal transduction pathway. *Mol Cell* **11**, 1479-89.

Lee, A. H., Iwakoshi, N. N. and Glimcher, L. H. (2003). XBP-1 regulates a subset of endoplasmic reticulum resident chaperone genes in the unfolded protein response. *Mol Cell Biol* **23**, 7448-59.

Lee, A. H., Scapa, E. F., Cohen, D. E. and Glimcher, L. H. (2008). Regulation of hepatic lipogenesis by the transcription factor XBP1. *Science* **320**, 1492-6.

Lee, K., Tirasophon, W., Shen, X., Michalak, M., Prywes, R., Okada, T., Yoshida, H., Mori, K. and Kaufman, R. J. (2002). IRE1-mediated unconventional mRNA splicing and S2P-mediated ATF6 cleavage merge to regulate XBP1 in signaling the unfolded protein response. *Genes Dev* **16**, 452-66.

Lee, S. Y., Reichlin, A., Santana, A., Sokol, K. A., Nussenzweig, M. C. and Choi, Y. (1997). TRAF2 is essential for JNK but not NF-κB activation and regulates lymphocyte proliferation and survival. *Immunity* **7**, 703-13.

Leonardi, A., Ellinger-Ziegelbauer, H., Franzoso, G., Brown, K. and Siebenlist, U. (2000). Physical and functional interaction of filamin (actin-binding protein-280) and tumor necrosis factor receptor-associated factor 2. *J Biol Chem* **275**, 271-8.

Lerner, A. G., Upton, J. P., Praveen, P. V., Ghosh, R., Nakagawa, Y., Igbaria, A., Shen, S., Nguyen, V., Backes, B. J., Heiman, M. et al. (2012). IRE1α induces thioredoxin-interacting protein to activate the NLRP3 inflammasome and promote programmed cell death under irremediable ER stress. *Cell Metab* **16**, 250-64.

Li, B., Yi, P., Zhang, B., Xu, C., Liu, Q., Pi, Z., Xu, X., Chevet, E. and Liu, J. (2011). Differences in endoplasmic reticulum stress signalling kinetics determine cell survival outcome through activation of MKP-1. *Cell Signal* **23**, 35-45.

Liu, J., Minemoto, Y. and Lin, A. (2004). c-Jun N-terminal protein kinase 1 (JNK1), but not JNK2, is essential for tumor necrosis factor alpha-induced c-Jun kinase activation and apoptosis. *Mol Cell Biol* **24**, 10844-56.

Lu, M., Lawrence, D. A., Marsters, S., Acosta-Alvear, D., Kimmig, P., Mendez, A. S., Paton, A. W., Paton, J. C., Walter, P. and Ashkenazi, A. (2014). Opposing unfolded-protein-response signals converge on death receptor 5 to control apoptosis. *Science* **345**, 98-101.

Massey, V. (1960). The identity of diaphorase and lipoyl dehydrogenase. *Biochim Biophys Acta* **37**, 314-22.

Mauro, C., Crescenzi, E., De Mattia, R., Pacifico, F., Mellone, S., Salzano, S., de Luca, C., D'Adamio, L., Palumbo, G., Formisano, S. et al. (2006). Central role of the scaffold protein tumor necrosis factor receptor-associated factor 2 in regulating endoplasmic reticulum stress-induced apoptosis. *J Biol Chem* **281**, 2631-8.

Mihai, A. D. and Schröder, M. (2015). Glucose starvation and hypoxia, but not the saturated fatty acid palmitic acid or cholesterol, activate the unfolded protein response in 3T3-F442A and 3T3-L1 adipocytes. *Adipocyte* **4**, 188-202.

Morton, H. J. (1970). A survey of commercially available tissue culture media. *In Vitro* **6**, 89-108.

Murphy, L. O., Smith, S., Chen, R. H., Fingar, D. C. and Blenis, J. (2002). Molecular interpretation of ERK signal duration by immediate early gene products. *Nat Cell Biol* **4**, 556-64.

Narita, M., Shimizu, S., Ito, T., Chittenden, T., Lutz, R. J., Matsuda, H. and Tsujimoto, Y. (1998). Bax interacts with the permeability transition pore to induce permeability transition and cytochrome *c* release in isolated mitochondria. *Proc Natl Acad Sci U S A* **95**, 14681-6.

Nishina, H., Fischer, K. D., Radvanyi, L., Shahinian, A., Hakem, R., Rubie, E. A., Bernstein, A., Mak, T. W., Woodgett, J. R. and Penninger, J. M. (1997). Stress-signalling kinase Sek1 protects thymocytes from apoptosis mediated by CD95 and CD3. *Nature* **385**, 350-3.

Nishitoh, H., Matsuzawa, A., Tobiume, K., Saegusa, K., Takeda, K., Inoue, K., Hori, S., Kakizuka, A. and Ichijo, H. (2002). ASK1 is essential for endoplasmic reticulum stress-induced neuronal cell death triggered by expanded polyglutamine repeats. *Genes Dev* **16**, 1345-55.

Novoa, I., Zhang, Y., Zeng, H., Jungreis, R., Harding, H. P. and Ron, D. (2003). Stress-induced gene expression requires programmed recovery from translational repression. *EMBO J* **22**, 1180-7.

Oda, Y., Okada, T., Yoshida, H., Kaufman, R. J., Nagata, K. and Mori, K. (2006). Derlin-2 and Derlin-3 are regulated by the mammalian unfolded protein response and are required for ER-associated degradation. *J Cell Biol* **172**, 383-93.

Oslowski, C. M., Hara, T., O'Sullivan-Murphy, B., Kanekura, K., Lu, S., Hara, M., Ishigaki, S., Zhu, L. J., Hayashi, E., Hui, S. T. et al. (2012). Thioredoxin-interacting protein mediates ER stress-induced β cell death through initiation of the inflammasome. *Cell Metab* **16**, 265-73.

Papa, S., Zazzeroni, F., Bubici, C., Jayawardena, S., Alvarez, K., Matsuda, S., Nguyen, D. U., Pham, C. G., Nelsbach, A. H., Melis, T. et al. (2004). Gadd45β

mediates the NF-κB suppression of JNK signalling by targeting MKK7/JNKK2. *Nat Cell Biol* **6**, 146-53.

Petrov, V. V., Smirnova, V. V. and Okorokov, L. A. (1992). Mercaptoethanol and dithiothreitol decrease the difference of electrochemical proton potentials across the yeast plasma and vacuolar membranes and activate their H^+-ATPases. *Yeast* **8**, 589-98.

Pfaffl, M. W. (2001). A new mathematical model for relative quantification in real-time RT-PCR. *Nucleic Acids Res* **29**, e45.

Prischi, F., Nowak, P. R., Carrara, M. and Ali, M. M. (2014). Phosphoregulation of Ire1 RNase splicing activity. *Nat Commun* **5**, 3554.

Rahmani, M., Peron, P., Weitzman, J., Bakiri, L., Lardeux, B. and Bernuau, D. (2001). Functional cooperation between JunD and NF-κB in rat hepatocytes. *Oncogene* **20**, 5132-42.

Raingeaud, J., Gupta, S., Rogers, J. S., Dickens, M., Han, J., Ulevitch, R. J. and Davis, R. J. (1995). Pro-inflammatory cytokines and environmental stress cause p38 mitogen-activated protein kinase activation by dual phosphorylation on tyrosine and threonine. *J Biol Chem* **270**, 7420-6.

Reers, M., Smith, T. W. and Chen, L. B. (1991). J-aggregate formation of a carbocyanine as a quantitative fluorescent indicator of membrane potential. *Biochemistry* **30**, 4480-6.

Reinhard, C., Shamoon, B., Shyamala, V. and Williams, L. T. (1997). Tumor necrosis factor α-induced activation of c-jun N-terminal kinase is mediated by TRAF2. *EMBO J* **16**, 1080-92.

Reuther-Madrid, J. Y., Kashatus, D., Chen, S., Li, X., Westwick, J., Davis, R. J., Earp, H. S., Wang, C.-Y. and Baldwin Jr, A. S., Jr. (2002). The p65/RelA subunit of NF-κB suppresses the sustained, antiapoptotic activity of Jun kinase induced by tumor necrosis factor. *Mol Cell Biol* **22**, 8175-83.

Ron, D. and Walter, P. (2007). Signal integration in the endoplasmic reticulum unfolded protein response. *Nat Rev Mol Cell Biol* **8**, 519-29.

Roulston, A., Reinhard, C., Amiri, P. and Williams, L. T. (1998). Early activation of c-Jun N-terminal kinase and p38 kinase regulate cell survival in response to tumor necrosis factor α. *J Biol Chem* **273**, 10232-9.

Rutzky, L. P. and Pumper, R. W. (1974). Supplement to a survey of commercially available tissue culture media (1970). *In Vitro* **9**, 468-9.

Sanchez-Perez, I., Murguia, J. R. and Perona, R. (1998). Cisplatin induces a persistent activation of JNK that is related to cell death. *Oncogene* **16**, 533-40.

Sandow, J. J., Dorstyn, L., O'Reilly, L. A., Tailler, M., Kumar, S., Strasser, A. and Ekert, P. G. (2014). ER stress does not cause upregulation and activation of caspase-2 to initiate apoptosis. *Cell Death Differ* **21**, 475-80.

Schimmer, A. D., Welsh, K., Pinilla, C., Wang, Z., Krajewska, M., Bonneau, M. J., Pedersen, I. M., Kitada, S., Scott, F. L., Bailly-Maitre, B. et al. (2004). Small-molecule antagonists of apoptosis suppressor XIAP exhibit broad antitumor activity. *Cancer Cell* **5**, 25-35.

Scorrano, L., Petronilli, V., Di Lisa, F. and Bernardi, P. (1999). Commitment to apoptosis by GD3 ganglioside depends on opening of the mitochondrial permeability transition pore. *J Biol Chem* **274**, 22581-5.

Shen, X., Ellis, R. E., Lee, K., Liu, C.-Y., Yang, K., Solomon, A., Yoshida, H., Morimoto, R., Kurnit, D. M., Mori, K. et al. (2001). Complementary signaling pathways regulate the unfolded protein response and are required for *C. elegans* development. *Cell* **107**, 893-903.

Shi, Y., An, J., Liang, J., Hayes, S. E., Sandusky, G. E., Stramm, L. E. and Yang, N. N. (1999). Characterization of a mutant pancreatic eIF-2α kinase, PEK, and co-localization with somatostatin in islet delta cells. *J Biol Chem* **274**, 5723-30.

Shi, Y., Vattem, K. M., Sood, R., An, J., Liang, J., Stramm, L. and Wek, R. C. (1998). Identification and characterization of pancreatic eukaryotic initiation factor 2 α-subunit kinase, PEK, involved in translational control. *Mol Cell Biol* **18**, 7499-509.

Šidák, Z. (1967). Rectangular confidence regions for the means of multivariate normal distributions. *J Am Stat Assoc* **62**, 626-33.

Sluss, H. K., Barrett, T., Derijard, B. and Davis, R. J. (1994). Signal transduction by tumor necrosis factor mediated by JNK protein kinases. *Mol Cell Biol* **14**, 8376-84.

Smiley, S. T., Reers, M., Mottola-Hartshorn, C., Lin, M., Chen, A., Smith, T. W., Steele, G. D., Jr. and Chen, L. B. (1991). Intracellular heterogeneity in mitochondrial membrane potentials revealed by a J-aggregate-forming lipophilic cation JC-1. *Proc Natl Acad Sci U S A* **88**, 3671-5.

Smith, M. I. and Deshmukh, M. (2007). Endoplasmic reticulum stress-induced apoptosis requires bax for commitment and Apaf-1 for execution in primary neurons. *Cell Death Differ* **14**, 1011-9.

Stehlik, C., de Martin, R., Kumabashiri, I., Schmid, J. A., Binder, B. R. and Lipp, J. (1998). Nuclear factor (NF)-κB-regulated X-chromosome-linked *iap* gene expression protects endothelial cells from tumor necrosis factor α-induced apoptosis. *J Exp Med* **188**, 211-6.

Tan, Y., Dourdin, N., Wu, C., De Veyra, T., Elce, J. S. and Greer, P. A. (2006). Ubiquitous calpains promote caspase-12 and JNK activation during endoplasmic reticulum stress-induced apoptosis. *J Biol Chem* **281**, 16016-24.

Tang, F., Tang, G., Xiang, J., Dai, Q., Rosner, M. R. and Lin, A. (2002). The absence of NF-κB-mediated inhibition of c-Jun N-terminal kinase activation contributes to tumor necrosis factor alpha-induced apoptosis. *Mol Cell Biol* **22**, 8571-9.

Tang, G., Minemoto, Y., Dibling, B., Purcell, N. H., Li, Z., Karin, M. and Lin, A. (2001). Inhibition of JNK activation through NF-κB target genes. *Nature* **414**, 313-7.

Teodoro, T., Odisho, T., Sidorova, E. and Volchuk, A. (2012). Pancreatic β-cells depend on basal expression of active ATF6α-p50 for cell survival even under nonstress conditions. *Am J Physiol Cell Physiol* **302**, C992-C1003.

Tirasophon, W., Welihinda, A. A. and Kaufman, R. J. (1998). A stress response pathway from the endoplasmic reticulum to the nucleus requires a novel bifunctional protein kinase/endoribonuclease (Ire1p) in mammalian cells. *Genes Dev* **12**, 1812-24.

Tournier, C., Hess, P., Yang, D. D., Xu, J., Turner, T. K., Nimnual, A., Bar-Sagi, D., Jones, S. N., Flavell, R. A. and Davis, R. J. (2000). Requirement of JNK for stress-induced activation of the cytochrome c-mediated death pathway. *Science* **288**, 870-4.

Traverse, S., Seedorf, K., Paterson, H., Marshall, C. J., Cohen, P. and Ullrich, A. (1994). EGF triggers neuronal differentiation of PC12 cells that overexpress the EGF receptor. *Curr Biol* **4**, 694-701.

Tukey, J. W. (1949). Comparing individual means in the analysis of variance. *Biometrics* **5**, 99-114.

Upton, J. P., Wang, L., Han, D., Wang, E. S., Huskey, N. E., Lim, L., Truitt, M., McManus, M. T., Ruggero, D., Goga, A. et al. (2012). IRE1α cleaves select

879 microRNAs during ER stress to derepress translation of proapoptotic caspase-2.
880 *Science* **338**, 818-22.
881 **Urano, F., Wang, X., Bertolotti, A., Zhang, Y., Chung, P., Harding, H. P. and**
882 **Ron, D.** (2000). Coupling of stress in the ER to activation of JNK protein kinases by
883 transmembrane protein kinase IRE1. *Science* **287**, 664-6.
884 **Ventura, J.-J., Cogswell, P., Flavell, R. A., Baldwin, A. S., Jr. and Davis, R. J.**
885 (2004). JNK potentiates TNF-stimulated necrosis by increasing the production of
886 cytotoxic reactive oxygen species. *Genes Dev* **18**, 2905-15.
887 **Ventura, J.-J., Hubner, A., Zhang, C., Flavell, R. A., Shokat, K. M. and Davis, R.**
888 **J.** (2006). Chemical genetic analysis of the time course of signal transduction by JNK.
889 *Mol Cell* **21**, 701-10.
890 **Ventura, J. J., Kennedy, N. J., Lamb, J. A., Flavell, R. A. and Davis, R. J.** (2003).
891 c-Jun NH_2-terminal kinase is essential for the regulation of AP-1 by tumor necrosis
892 factor. *Mol Cell Biol* **23**, 2871-82.
893 **Vince, J. E., Chau, D., Callus, B., Wong, W. W., Hawkins, C. J., Schneider, P.,**
894 **McKinlay, M., Benetatos, C. A., Condon, S. M., Chunduru, S. K. et al.** (2008).
895 TWEAK-FN14 signaling induces lysosomal degradation of a cIAP1-TRAF2 complex
896 to sensitize tumor cells to TNFα. *J Cell Biol* **182**, 171-84.
897 **Vince, J. E., Wong, W. W., Khan, N., Feltham, R., Chau, D., Ahmed, A. U.,**
898 **Benetatos, C. A., Chunduru, S. K., Condon, S. M., McKinlay, M. et al.** (2007).
899 IAP antagonists target cIAP1 to induce TNFα-dependent apoptosis. *Cell* **131**, 682-93.
900 **Walter, P. and Ron, D.** (2011). The unfolded protein response: from stress pathway
901 to homeostatic regulation. *Science* **334**, 1081-6.
902 **Wang, Q., Zhang, H., Zhao, B. and Fei, H.** (2009). IL-1β caused pancreatic β-cells
903 apoptosis is mediated in part by endoplasmic reticulum stress via the induction of
904 endoplasmic reticulum Ca^{2+} release through the c-Jun N-terminal kinase pathway.
905 *Mol Cell Biochem* **324**, 183-90.
906 **Wang, X. Z., Harding, H. P., Zhang, Y., Jolicoeur, E. M., Kuroda, M. and Ron,**
907 **D.** (1998). Cloning of mammalian Ire1 reveals diversity in the ER stress responses.
908 *EMBO J* **17**, 5708-17.
909 **Whitesides, G. M., Lilburn, J. E. and Szajewski, R. P.** (1977). Rates of thiol-
910 disulfide interchange reactions between mono- and dithiols and Ellman's reagent. *J*
911 *Org Chem* **42**, 332-8.

Wu, S., Hu, Y., Wang, J. L., Chatterjee, M., Shi, Y. and Kaufman, R. J. (2002). Ultraviolet light inhibits translation through activation of the unfolded protein response kinase PERK in the lumen of the endoplasmic reticulum. *J Biol Chem* **277**, 18077-83.

Wu, S., Tan, M., Hu, Y., Wang, J. L., Scheuner, D. and Kaufman, R. J. (2004). Ultraviolet light activates NFκB through translational inhibition of IκBα synthesis. *J Biol Chem* **279**, 34898-902.

Yang, Q.-H. and Du, C. (2004). Smac/DIABLO selectively reduces the levels of c-IAP1 and c-IAP2 but not that of XIAP and livin in HeLa cells. *J Biol Chem* **279**, 16963-70.

Yeh, W.-C., Shahinian, A., Speiser, D., Kraunus, J., Billia, F., Wakeham, A., de la Pompa, J. L., Ferrick, D., Hum, B., Iscove, N. et al. (1997). Early lethality, functional NF-κB activation, and increased sensitivity to TNF-induced cell death in TRAF2-deficient mice. *Immunity* **7**, 715-25.

Yoneda, T., Imaizumi, K., Oono, K., Yui, D., Gomi, F., Katayama, T. and Tohyama, M. (2001). Activation of caspase-12, an endoplastic reticulum (ER) resident caspase, through tumor necrosis factor receptor-associated factor 2-dependent mechanism in response to the ER stress. *J Biol Chem* **276**, 13935-40.

Yoshida, H., Matsui, T., Hosokawa, N., Kaufman, R. J., Nagata, K. and Mori, K. (2003). A time-dependent phase shift in the mammalian unfolded protein response. *Dev Cell* **4**, 265-71.

Yoshida, H., Matsui, T., Yamamoto, A., Okada, T. and Mori, K. (2001). XBP1 mRNA is induced by ATF6 and spliced by IRE1 in response to ER stress to produce a highly active transcription factor. *Cell* **107**, 881-91.

Yoshida, H., Okada, T., Haze, K., Yanagi, H., Yura, T., Negishi, M. and Mori, K. (2000). ATF6 activated by proteolysis binds in the presence of NF-Y (CBF) directly to the *cis*-acting element responsible for the mammalian unfolded protein response. *Mol Cell Biol* **20**, 6755-67.

Yu, C., Minemoto, Y., Zhang, J., Liu, J., Tang, F., Bui, T. N., Xiang, J. and Lin, A. (2004). JNK suppresses apoptosis via phosphorylation of the proapoptotic Bcl-2 family protein BAD. *Mol Cell* **13**, 329-40.

Zhang, C., Kawauchi, J., Adachi, M. T., Hashimoto, Y., Oshiro, S., Aso, T. and Kitajima, S. (2001). Activation of JNK and transcriptional repressor ATF3/LRF1

through the IRE1/TRAF2 pathway is implicated in human vascular endothelial cell death by homocysteine. *Biochem Biophys Res Commun* **289**, 718-24.

Zhang, K., Shen, X., Wu, J., Sakaki, K., Saunders, T., Rutkowski, D. T., Back, S. H. and Kaufman, R. J. (2006). Endoplasmic reticulum stress activates cleavage of CREBH to induce a systemic inflammatory response. *Cell* **124**, 587-99.

Figure Legends

Fig. 1. JNK activation precedes activation of *XBP1* splicing in MEFs. **(A)** Kinetics of JNK and eIF2α phosphorylation and **(B)** *XBP1* splicing in MEFs exposed to 1 μM thapsigargin. **(C)** Quantification of JNK (white circles, solid line, $n = 4$) and eIF2α (white squares, dotted line) phosphorylation from panel (A) and of *XBP1* splicing (black circles, dashed line, $n = 2$) from panel (B). **(D)** Kinetics of JNK and eIF2α phosphorylation and **(E)** *XBP1* splicing in MEFs exposed to 10 μg/ml tunicamycin. **(F)** Quantification of JNK (white circles, solid line, $n = 3$) and eIF2α (white squares, dotted line) phosphorylation from panel (D) and of *XBP1* splicing (black circles, dashed line) from panel (E). *p* values for comparison of the JNK phosphorylation after addition of the drugs to the cells to JNK phosphorylation in the untreated cells were obtained from an ordinary one way analysis of variance (ANOVA) with Dunnett's correction for multiple comparisons (Dunnett, 1955; Dunnett, 1964). * - $p < 0.05$, ** - $p < 0.01$, *** - $p < 0.001$, and **** - $p < 0.0001$. A repeat of the eIF2α Western blots gave qualitatively similar results.

Fig. 2. IRE1α and TRAF2 are required for the initial phase of JNK activation in MEFs. **(A)** Kinetics of JNK and eIF2α phosphorylation and **(B)** *XBP1* splicing in *ire1α*$^{-/-}$ MEFs exposed to 1 μM thapsigargin. For eIF2α phosphorylation qualitatively similar data were obtained in one repeat of the experiment. **(C)** Quantification of JNK (white circles, solid line, $n = 3$) and eIF2α (white squares, dotted line) phosphorylation from panel (A) and of *XBP1* splicing (black circles, dashed line) from panel (B). **(D)** Kinetics of JNK and eIF2α phosphorylation and **(E)** *XBP1* splicing in *traf2*$^{-/-}$ MEFs exposed to 1 μM thapsigargin. eIF2α phosphorylation was expressed relative to the 480 min time point. **(F)** Quantification of JNK (white circles, solid line, $n = 3$) and eIF2α phosphorylation (white squares, dotted line, $n = 2$) from panel (D) and *XBP1* splicing (black circles, dashed line) from panel (E). **(G)** Comparison of phosphorylation of JNK in WT, *ire1α*$^{-/-}$, and *traf2*$^{-/-}$ MEFs before the onset of elevated JNK phosphorylation after 240 min of ER stress in *ire1α*$^{-/-}$ and

978 *traf2*$^{-/-}$ MEFs. The bars represent the relative JNK phosphorylation before, 10, 20, 30,
979 45, 60, 120, and 240 min after addition of thapsigargin to the cells. *p* values for
980 comparison of JNK phosphorylation in treated cells to the JNK phosphorylation in
981 untreated cells were calculated with an ordinary one way ANOVA with Dunnett's
982 correction for multiple comparisons.
983 **Fig. 3.** JNK inhibits cell death early in the ER stress response. **(A)** WT and *jnk1*$^{-/-}$
984 *jnk2*$^{-/-}$ MEFs were treated with 1 μM thapsigargin (Tg) or 10 μg/ml tunicamycin (Tm)
985 for 4 h and stained with JC-1 as described in Materials and Methods. Scale bar – 10
986 μm. **(B, C)** Quantification of the confocal fluorescence microscopy data shown in
987 panel A for (B) thapsigargin- and (C) tunicamycin-treated cells. At least 600 cells
988 were counted for each sample. (**D**) Combined activities of caspases 3 and 7 in WT and
989 *jnk1*$^{-/-}$ *jnk2*$^{-/-}$ MEFs treated for 4 h with 1 or 2 μM thapsigargin (Tg) or **(E)** 10 μg/ml
990 tunicamycin (Tm). The combined caspase activities are expressed relative to the
991 untreated cells. *p* values were calculated with an ordinary two way ANOVA with
992 Šidák's correction for multiple comparisons (Šidák, 1967) (n = 3 for panels D and E).
993 **Fig. 4.** JNK is required for transcriptional induction of antiapoptotic genes early in the
994 ER stress response. **(A)** *cIAP1* (*BIRC2*), **(B)** *cIAP2* (*BIRC3*), **(C)** *XIAP* (*BIRC4)*, and
995 **(D)** *BIRC6* (*BRUCE*) steady-state mRNA levels were quantified by RT-qPCR in WT
996 and *jnk1*$^{-/-}$ *jnk2*$^{-/-}$ MEFs exposed to 1 μM thapsigargin for the indicated times. The *p*
997 values for the genotype comparisons of an ordinary two way ANOVA with Šidák's
998 correction for multiple comparisons are shown (n = 3).
999 **Fig. 5.** cIAP1, cIAP2, and XIAP protect against apoptosis early in the ER stress
1000 response. **(A)** Combined activities of caspases 3 and 7 in untreated WT, *ciap1*$^{-/-}$
1001 *ciap2*$^{-/-}$, and *xiap*$^{-/-}$ MEFs and after exposure to **(B)** 2 μM thapsigargin (Tg) or **(C)** 10
1002 μg/ml tunicamycin (Tm) for 4 h. *p* values were calculated with an ordinary two way
1003 ANOVA with Dunnett's (panel A) or Tukey's (Tukey, 1949) (panels B and C)
1004 correction for multiple comparisons (n = 3).
1005 **Fig. 6.** Immediately activated JNK localizes to the cytosol during ER stress. Serum-
1006 starved Hep G2 cells were treated for 45 min with 1 μM thapsigargin or left untreated
1007 before isolation of the cytosolic and nuclear fractions. The cytosolic (C) and nuclear
1008 (N) fractions were analysed by Western blotting. The asterisk (*) indicates a non-
1009 specific band recognised by the anti-emerin antibody. Emerin was used as a nuclear

marker and GAPDH as a cytoplasmic marker. The experiment was repeated once with qualitatively similar results.

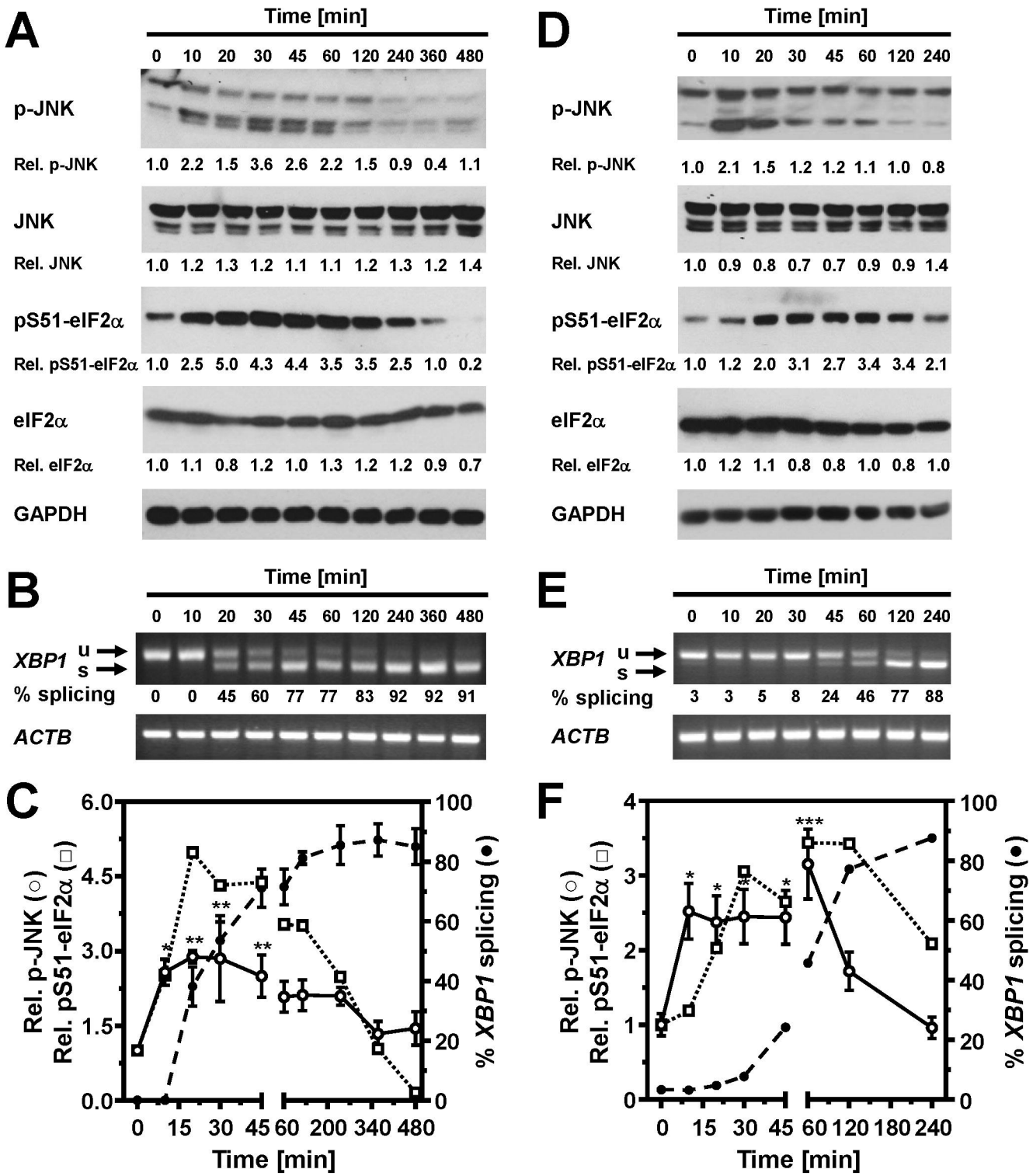

Figure 1, Brown *et al.*

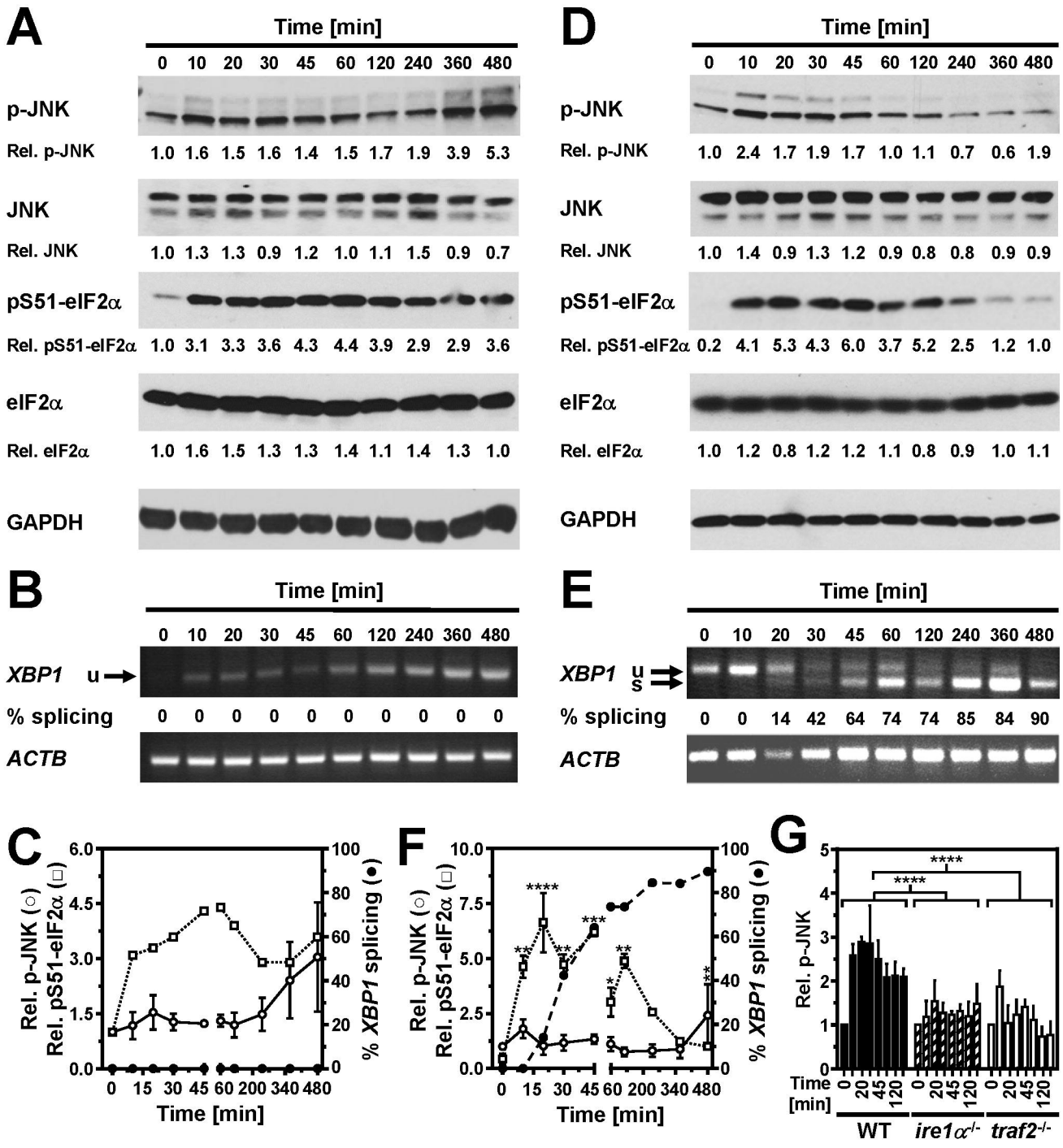

Figure 2, Brown *et al.*

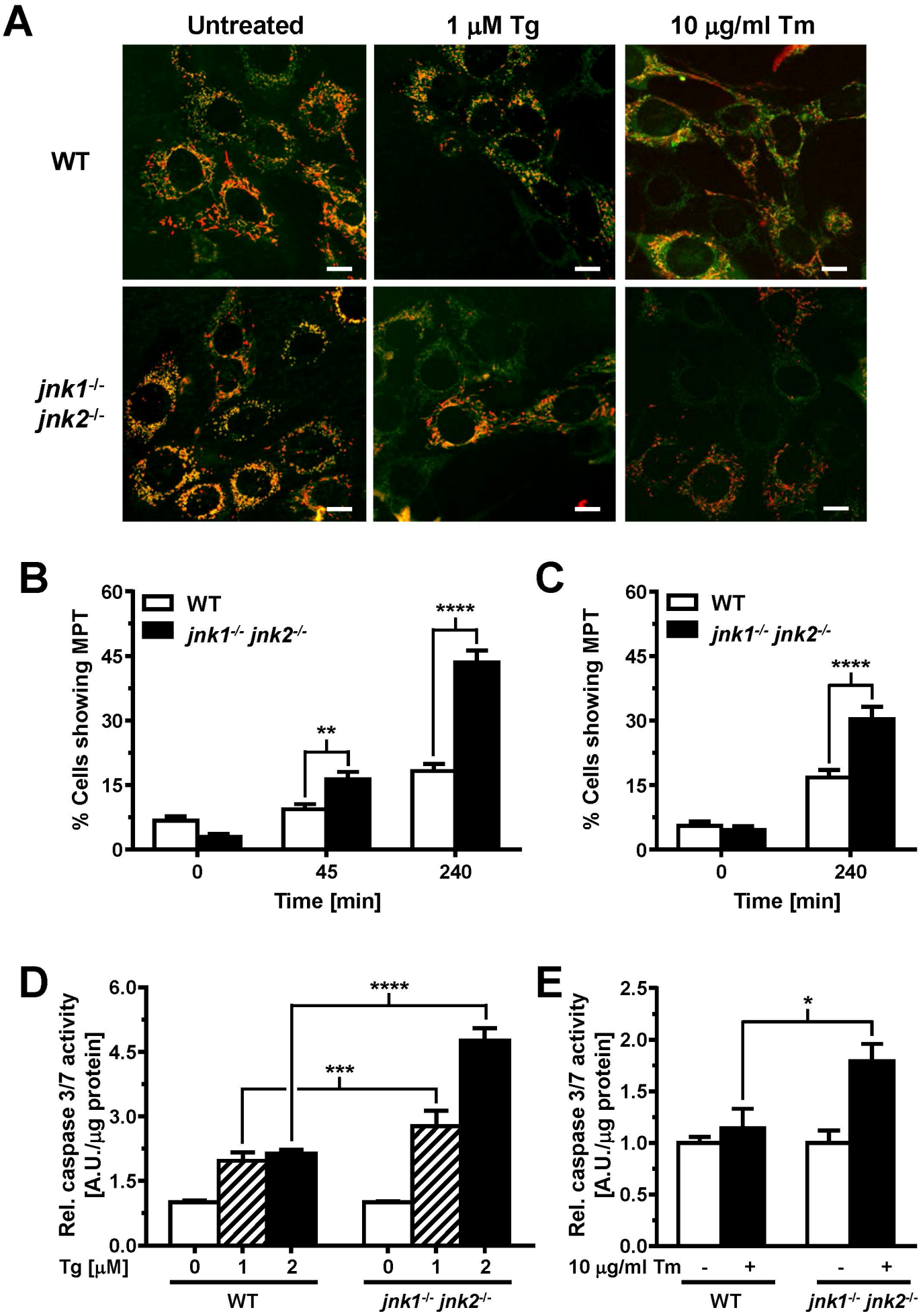

Figure 3, Brown *et al.*

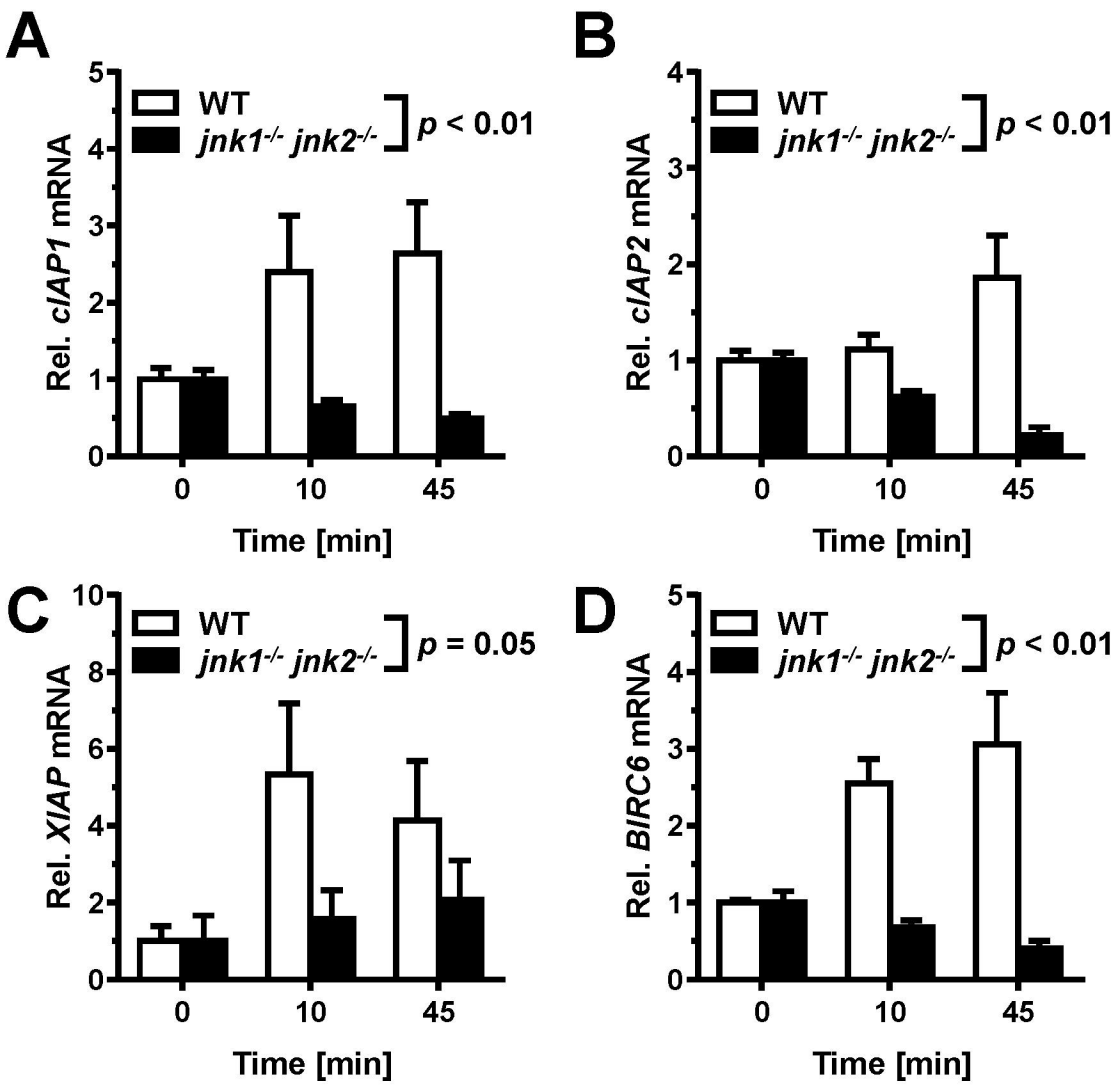

Figure 4, Brown *et al.*

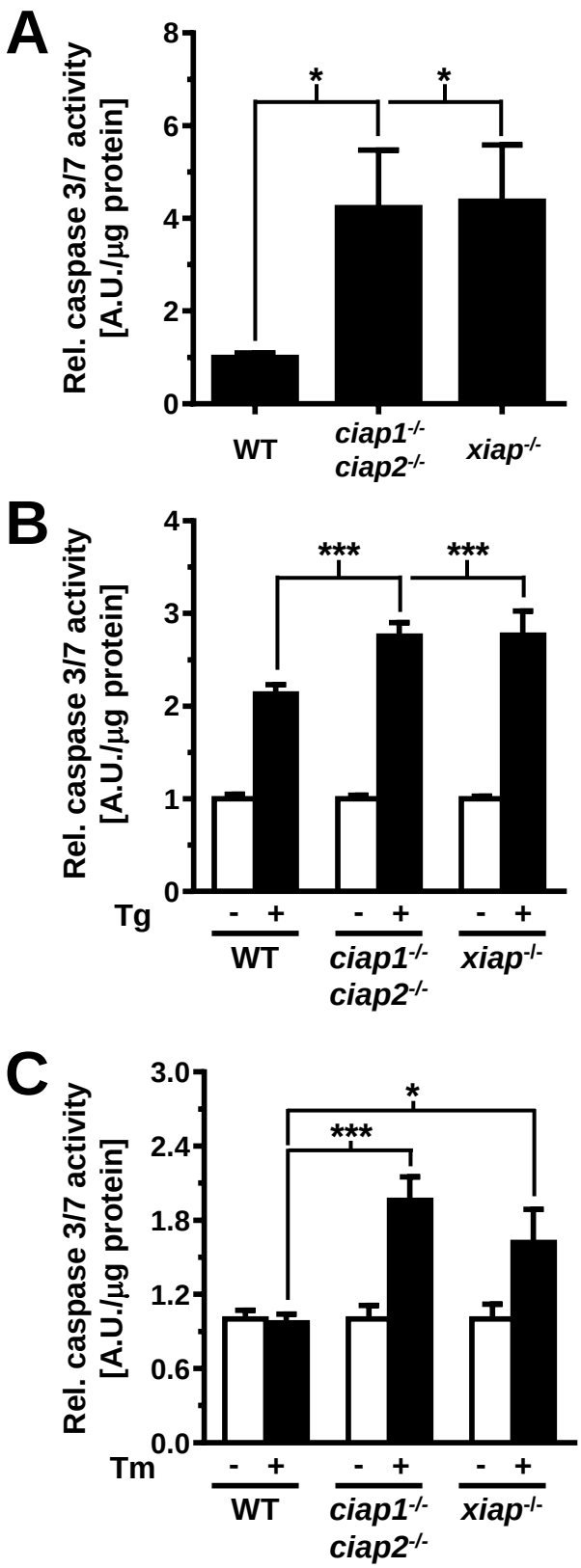

Figure 5, Brown *et al.*

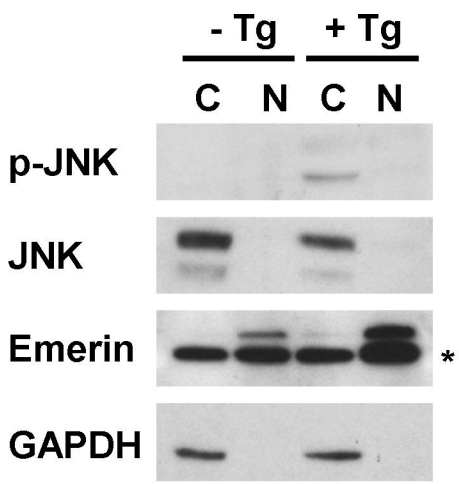

Figure 6, Brown *et al.*

Supplemental figure legends

Fig. S1. Kinetics of JNK and eIF2α phosphorylation and of *XBP1* splicing in response to acute ER stress in (A-C) Hep G2 cells, (D-F) *in vitro* differentiated 3T3-F442A adipocytes, and (G-J) *in vitro* differentiated C_2C_{12} myotubes. **(A)** Western blots for phospho-S51-eIF2α (pS51-eIF2α), eIF2α, phospho-JNK (p-JNK), JNK, and GAPDH and **(B)** *XBP1* splicing in Hep G2 cells exposed to 1 μM thapsigargin for the indicated times. **(C)** Quantification of the JNK (white circles, solid line, $n = 3$) and eIF2α phosphorylation (white squares, dotted line) from panel (A) and of *XBP1* splicing (black circles, dashed line) from panel (B). **(D)** Western blots for pS51-eIF2α, eIF2α, p-JNK, JNK, GAPDH and **(E)** *XBP1* splicing in 3T3-F442A cells exposed to 1 μM thapsigargin for the indicated times. **(F)** Quantification of JNK (white circles, solid line, $n = 2$) and eIF2α (white squares, dotted line) phosphorylation from panel (D) and *XBP1* splicing (black circles, dashed line) from panel (E). **(G)** mRNA levels for the muscle differentiation markers *AHCY* encoding *S*-adenosyl-homocysteine hydrolase, *MYL1* encoding myosin light chain 1, and *TNNC1* encoding troponin C in differentiated C_2C_{12} cells. The fold changes in mRNA abundance relative to undifferentiated cells (day 0) are shown. **(H)** Western blots for pS51-eIF2α, eIF2α, p-JNK, JNK, and GAPDH and **(I)** *XBP1* splicing in C_2C_{12} cells exposed to 1 μM thapsigargin for the indicated times. **(J)** Quantification of JNK (white circles, solid line, $n = 2$) and eIF2α (white squares, dotted line, $n = 2$) phosphorylation from panel (H) and of *XBP1* splicing (black circles, dashed line) from panel (I). *p* values for comparison of the JNK phosphorylation in treated to the JNK phosphorylation in untreated cells were calculated with an ordinary one way ANOVA with Dunnett's correction for multiple comparisons. A repeat of each eIF2α Western blot gave qualitatively similar results.

Fig. S2. The initial phase of JNK activation requires IRE1α and TRAF2 in Hep G2 cells. **(A)** Hep G2 cells were transfected with 10 nM of the indicated siRNAs against human *IRE1α*. 48 h and 72 h after transfection *IRE1α* mRNA was quantified by RT-qPCR. **(B)** siRNA knock-down of IRE1α impairs ER stress-dependent activation of JNK in Hep G2 cells. 72 h after transfection with the indicated siRNAs Hep G2 cells were stimulated for the indicated times with 1 μM thapsigargin. Cell lysates were analysed by Western blotting. **(C)** Quantification of JNK phosphorylation in Hep G2 cells treated for the indicated times with 1 μM thapsigargin 72 h after transfection with the indicated siRNAs. The average and s.e.m. from two independent experiments are shown. *p* values for comparison of the relative JNK

phosphorylation in cells transfected with *eGFP* and *hIRE1α* siRNAs at 2 and 4 h were calculated by using an ordinary two way ANOVA test with Tukey's correction for multiple comparisons. **(D)** siRNA knock-down of human TRAF2 in Hep G2 cells. Relative *TRAF2* mRNA abundance (to *ACTA1*) was measured by RT-qPCR 24 or 48 h after transfection of Hep G2 cells with the indicated siRNAs. **(E)** Knock-down of TRAF2 expression in Hep G2 cells interferes with ER stress-induced JNK phosphorylation. Hep G2 cells were treated with 1 μM thapsigargin for the times indicated before protein extraction for Western blotting with antibodies against p-JNK, JNK2, TRAF2, and GAPDH. **(F)** Quantification of the JNK phosphorylation signals in the Western blots of panel (E).

Fig. S3. The initial phase of JNK activation is TRAF2-dependent in 3T3-F442A preadipocytes and in C_2C_{12} myoblasts. **(A, B)** *TRAF2* mRNA levels measured by real-time PCR in (A) 3T3-F442A preadipocytes and (B) C_2C_{12} myoblasts after transfection with the indicated siRNAs. **(C)** TRAF2 protein levels relative to GAPDH in 3T3-F442A preadipocytes transfected with the indicated siRNAs against eGFP or murine TRAF2. Cells were treated with 20 ng/ml TNF-α for 20 min where indicated. **(D)** JNK phosphorylation and **(E)** *XBP1* splicing in 3T3-F442A preadipocytes transfected with a siRNA against eGFP. **(F)** Quantification of the JNK phosphorylation (white circles, solid line) from panel (D) and *XBP1* splicing (black circles, dashed line) from panel (E). **(G)** JNK phosphorylation and **(H)** *XBP1* splicing in 3T3-F442A preadipocytes transfected with murine *TRAF2* siRNA #2. **(I)** Quantification of the JNK phosphorylation (white circles, solid line, $n = 3$) from panel (G) and *XBP1* splicing (black circles, dashed line, $n = 2$) from panel (H). **(J)** JNK phosphorylation and **(K)** *XBP1* splicing in C_2C_{12} myoblasts transfected with control siRNA against eGFP. (**L)** Quantification of the JNK phosphorylation (white circles, solid line, $n = 2$) from panel (J) and *XBP1* splicing (black circles, dashed line, $n = 2$) from panel (K). **(M)** JNK phosphorylation and **(N)** *XBP1* splicing in C_2C_{12} myoblasts transfected with murine *TRAF2* siRNA #2. **(O)** Quantification of the JNK phosphorylation (white circles, solid line, $n = 3$) from panel (M) and *XBP1* splicing (black circles, dashed line) from panel (N). *p* values for comparison of the JNK phosphorylation in treated to the JNK phosphorylation in untreated cells were calculated with an ordinary one way ANOVA with Dunnett's correction for multiple comparisons.

Fig. S4. Dominant negative TRAF2 blocks initial JNK activation by ER stress in 3T3-F442A preadipocytes (C-D) and C_2C_{12} myotubes (E-F). **(A)** Domain structures of WT and dominant-negative TRAF2 (TRAF2Δ1-86). **(B)** Western blots for phospho-JNK, JNK2, and TRAF2 in

cell lysates prepared from WT and *traf2*$^{-/-}$ MEFs transiently transfected with 8 μg pMT2T-TRAF2Δ1-86 and stimulated with 50 ng/ml TNF-α for 20 min where indicated. **(C)** JNK phosphorylation in 3T3-F442A preadipocytes transfected with pMT2T-TRAF2Δ1-86 to express dominant-negative TRAF2Δ1-86. **(D)** Quantification of the JNK phosphorylation signals in the Western blots of panel (C). **(E)** JNK phosphorylation in C_2C_{12} myoblasts transfected with pMT2T-TRAF2Δ1-86 to express dominant-negative TRAF2Δ1-86. **(F)** Quantification of the JNK phosphorylation signals.

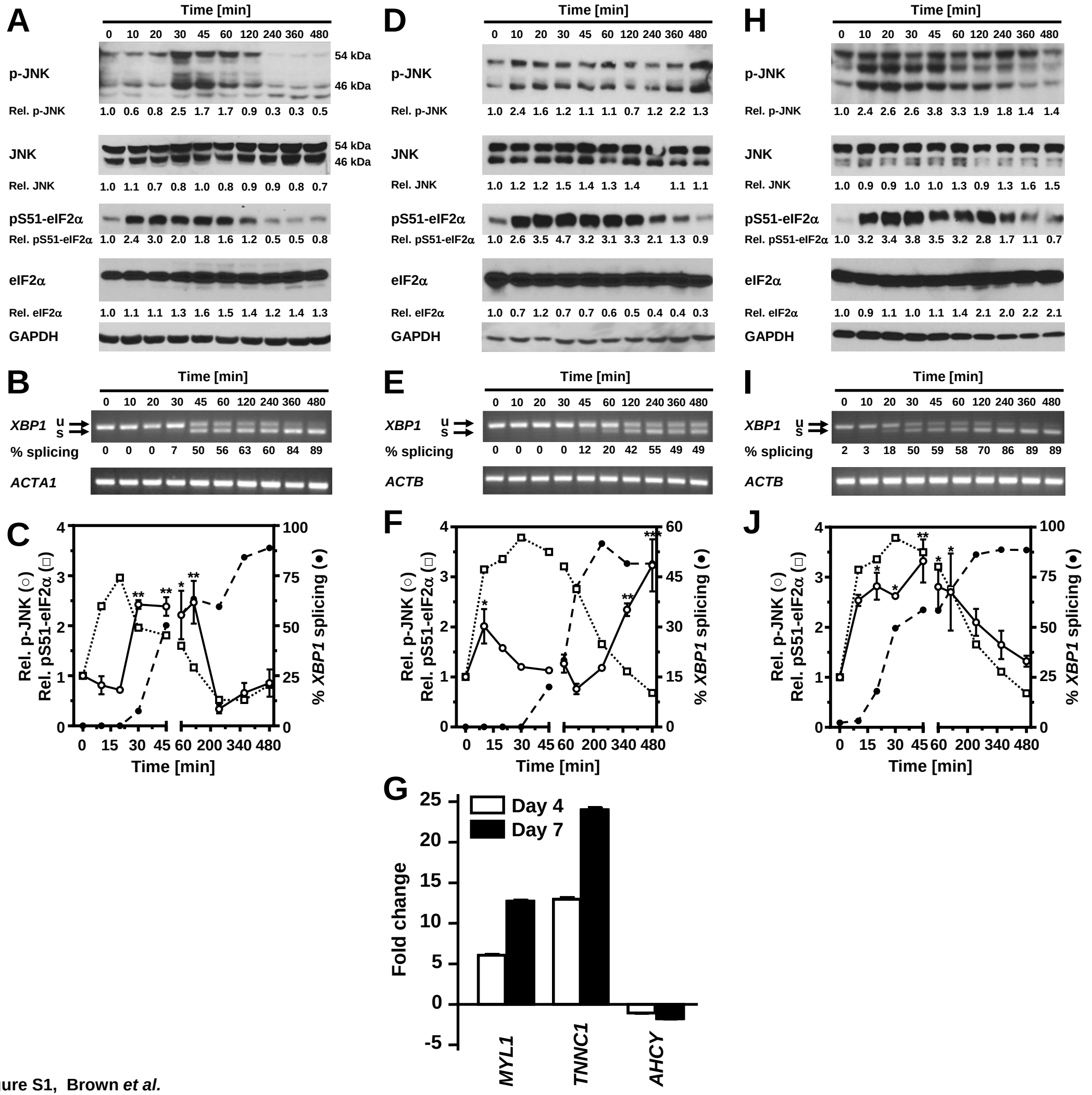

Figure S1, Brown *et al.*

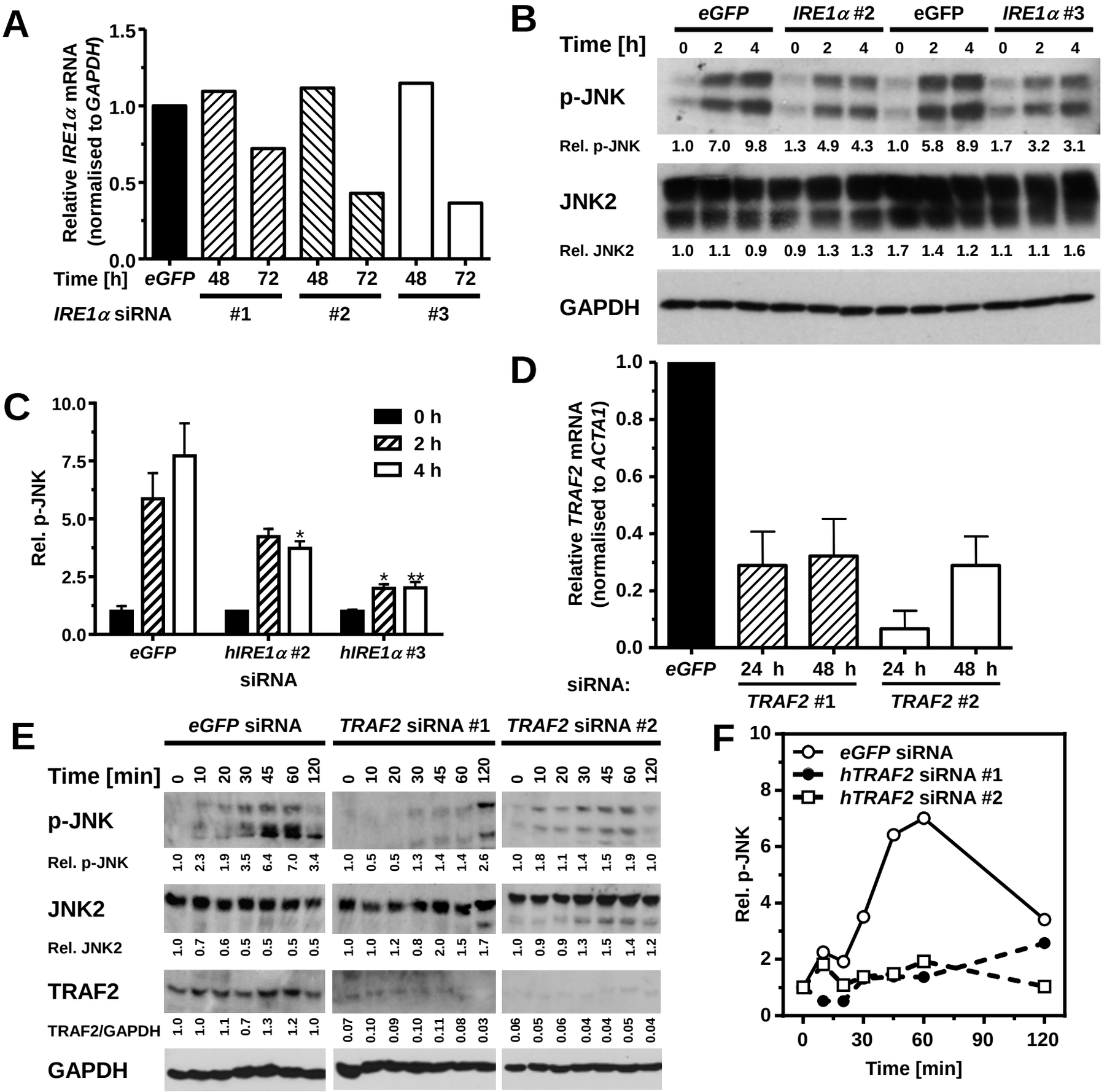

Figure S2, Brown *et al.*

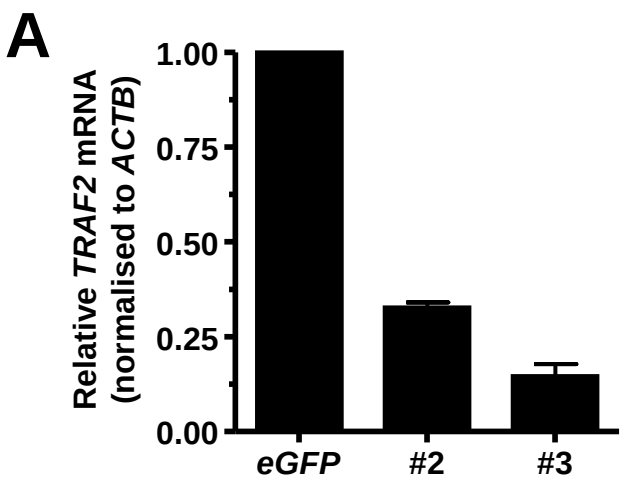

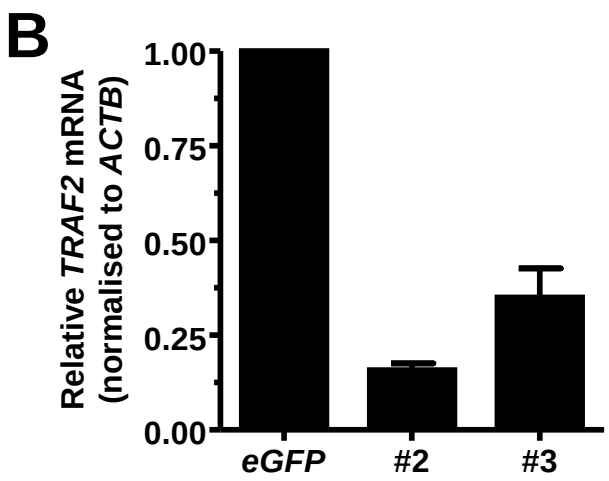

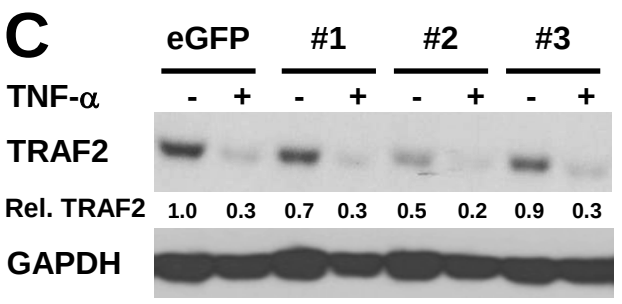

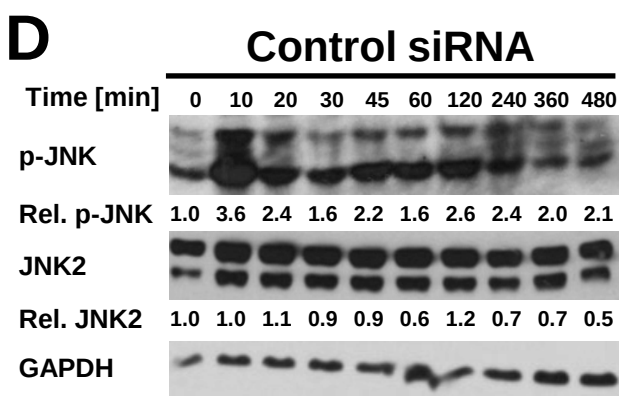

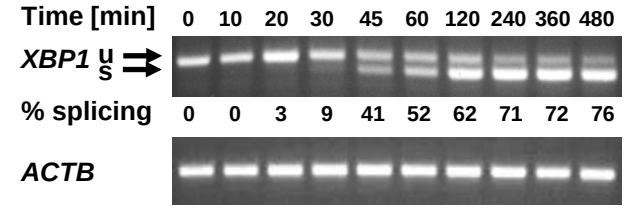

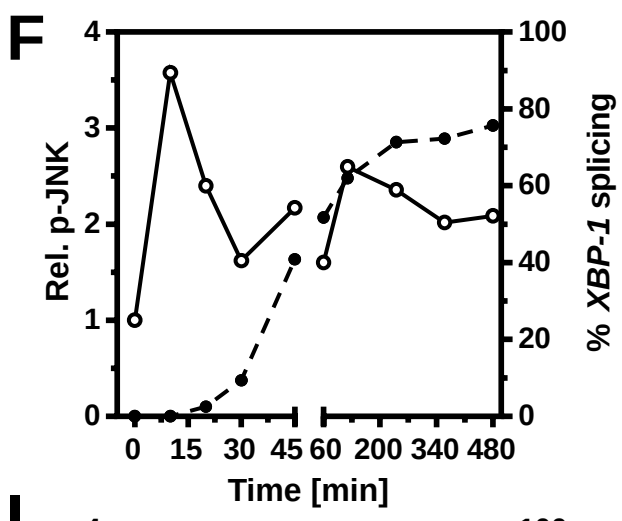

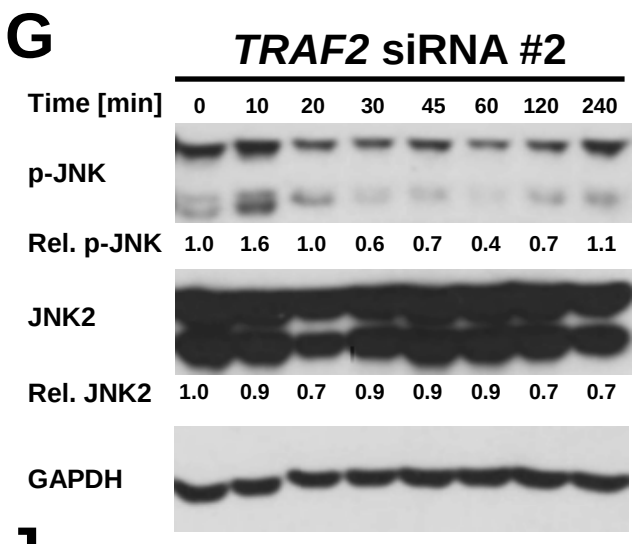

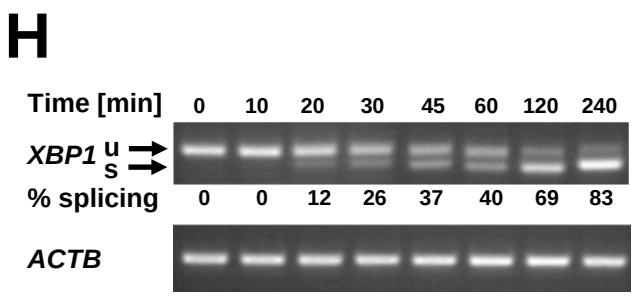

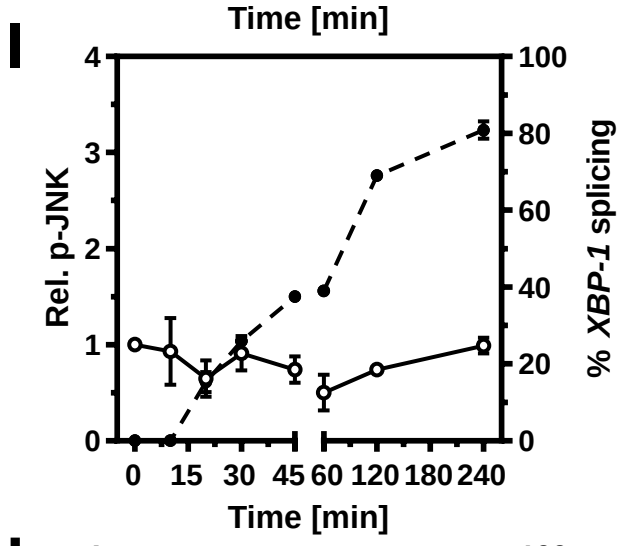

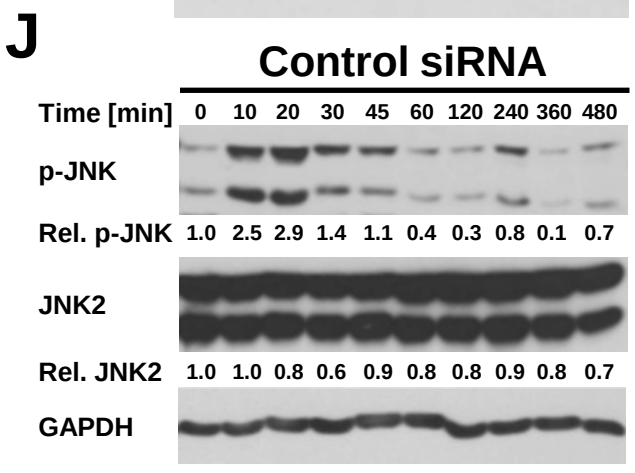

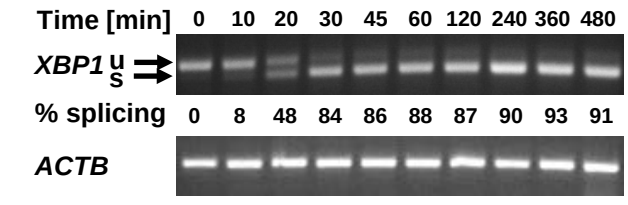

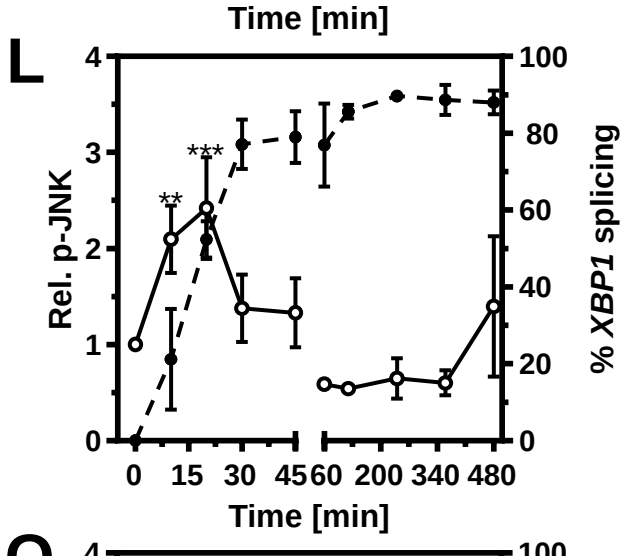

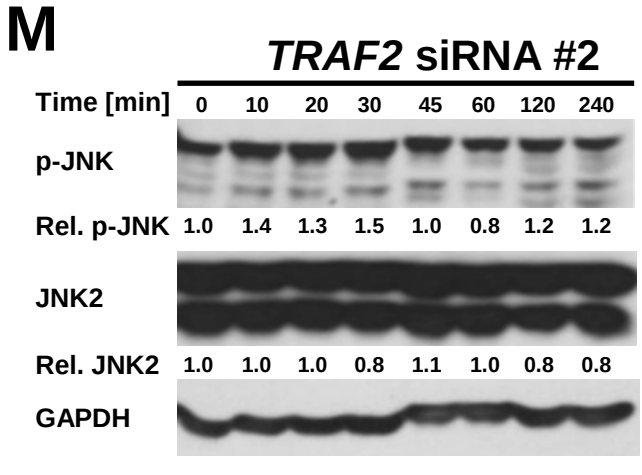

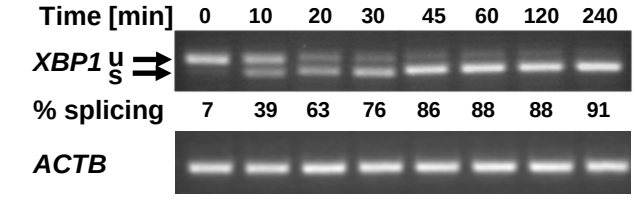

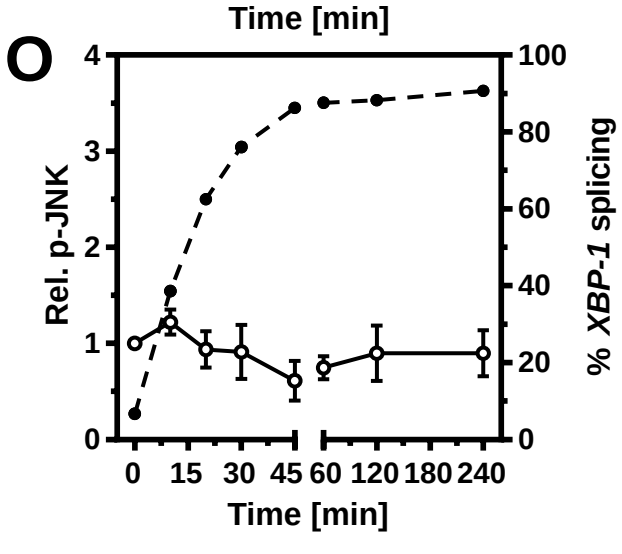

Figure S3, Brown *et al.*

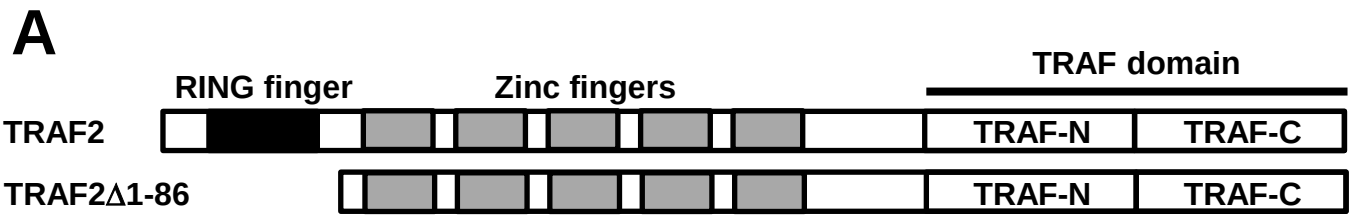

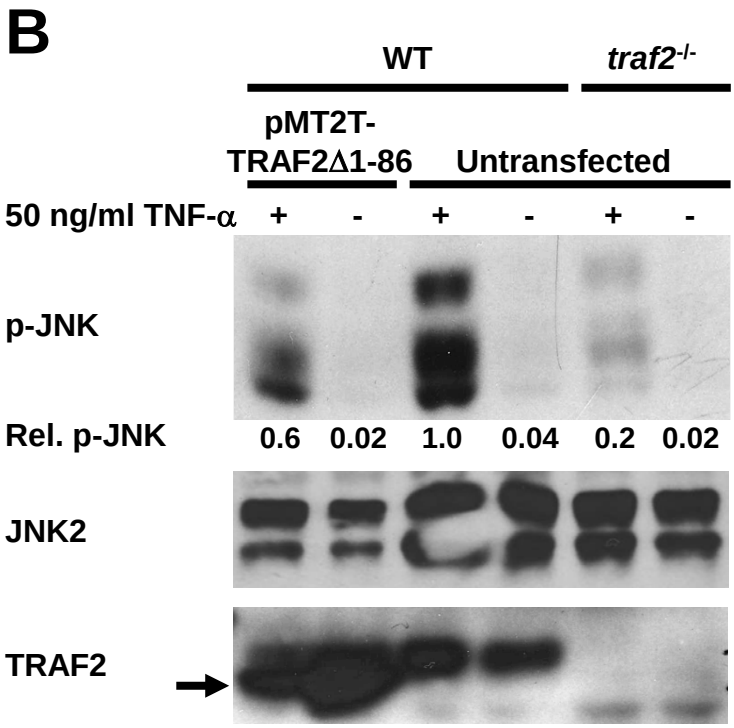

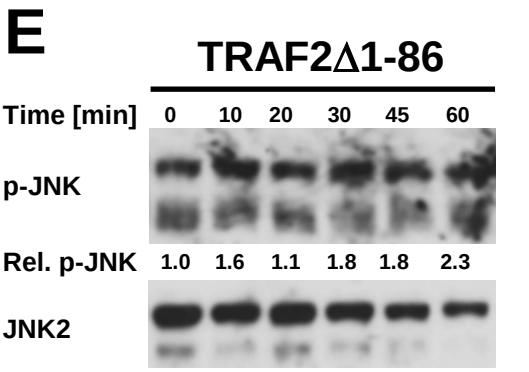

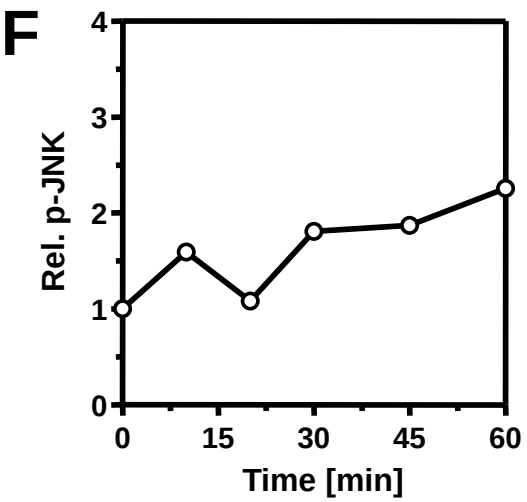

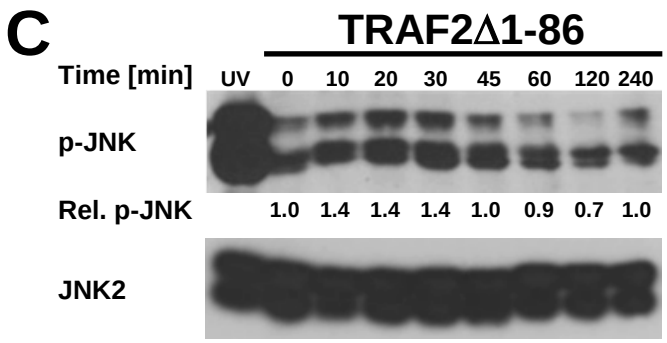

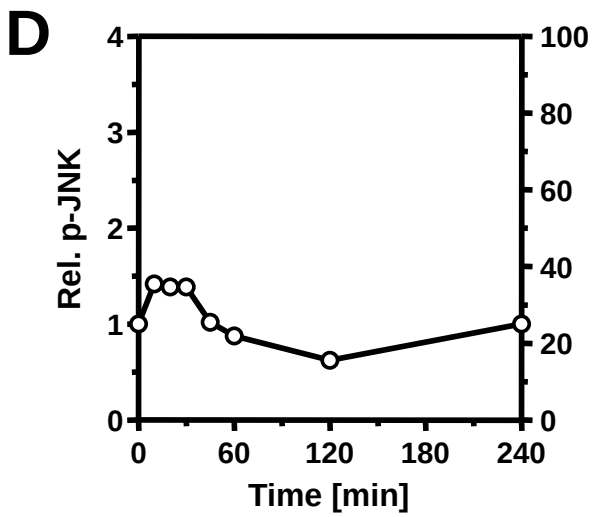

Figure S4, Brown *et al.*

Table S1. siRNAs.

Species	Gene	#	Sequence
Homo sapiens	*IRE1α*	1	GCGUAAAUUCAGGACCUAUdTdT
H. sapiens	*IRE1α*	2	GAUAGUCUCUGCCCAUCAAdTdT
H. sapiens	*IRE1α*	3	CAUUGCACGUGAAUUGAUAdTdT
H. sapiens	*TRAF2*	1	CACUCAGAGUGGGAGCACAdTdT
H. sapiens	*TRAF2*	2	GUCAAGACUUGUGGCAAGUdTdT
H. sapiens	*TRAF2*	3	GCCUUCAGGCCCGACGUGAdTdT
Mus musculus	*TRAF2*	1	GAAUUCCUAUGUGCGGGAUdTdT
M. musculus	*TRAF2*	2	GUUAGAGCAUGCAGCAAAUdTdT
M. musculus	*TRAF2*	3	CTATGAAGGCCTGTATGAAdTdT
Aequora victora	eGFP		GCAAGCUGACCCUGAAGUUCAU

Table S2. Oligodeoxynucleotides. Restriction sites are underlined. The start codon for TRAF2Δ1-86 is shown in bold.

Name	Purpose	Sequence
Oligodeoxynucleotides for *H. sapiens* genes		
H8197	*TRAF2* RT-qPCR for siRNA #3, reverse	AATGGCCTTGATGAAGATGG
H8215	*TRAF2Δ1-86* construction, forward primer	TGCATCGAT**ATG**AGCAGTTCGGCCTTCCCA
H8216	*TRAF2Δ1-86* construction, reverse primer	CGAGCGGCCGCCACTGTGCTGGATATCTGC
H8280	*TRAF2* RT-qPCR for siRNA #1, forward	CTTAGCCAAGGGCTGTGGT
H8281	*TRAF2* RT-qPCR for siRNA #1, reverse	AGGAATGCTCCCTTCTCTCC
H8282	*TRAF2* RT-qPCR for siRNA #2, forward	GTCCGCCTTGGTGAAAAG
H8283	*TRAF2* RT-qPCR for siRNA #2, reverse	TCTCACCCTCTACCGTCTCG
H8284	*TRAF2* RT-qPCR for siRNA #3, forward	ACACCAGCAGGTACGGCTAC
H8285	*GAPDH* RT-qPCR, forward	TCACCAGGGCTGCTTTTAAC
H8286	*GAPDH* RT-qPCR, reverse	GGCAGAGATGATGACCCTTT
H8287	*ACTA1* RT-qPCR, forward	CTGAGCGTGGCTACTCCTTC
H8288	*ACTA1* RT-qPCR, reverse	GGCATACAGGTCCTTCCTGA
H8289	*XBP1* PCR, forward	GAGTTAAGACAGCGCTTGGG
H8290	*XBP1* PCR, reverse	ACTGGGTCCAAGTTGTCCAG
H8993	*IRE1α* RT-qPCR, forward	TGGGACAGCTAGGCTGAGAT
H8994	*IRE1α* RT-qPCR, reverse	TGGGCACATCTGTGATCAAT
Oligodeoxynucleotides for *M. musculus* genes		
H7961	*XBP1* PCR, forward	GATCCTGACGAGGTTCCAGA
H7962	*XBP1* PCR, reverse	ACAGGGTCCAACTTGTCCAG
H7994	*ACTB* PCR, forward	AGCCATGTACGTAGCCATCC
H7995	*ACTB* PCR, reverse	CTCTCAGCTGTGGTGGTGAA

H8237	*TRAF2* RT-qPCR for siRNA #1, forward	GAACTCATCTGTCTCTCTTCTTCG
H8238	*TRAF2* RT-qPCR for siRNA #1, reverse	AGCAGGGGTGGCTAGAGTCC
H8239	*TRAF2* RT-qPCR for siRNA #2, forward	CTGCAGAGCACCCTGTAGC
H8240	*TRAF2* RT-qPCR for siRNA #2, reverse	CCTGCAGGTTCTCAGTCTCC
H8269	*TRAF2* RT-qPCR for siRNA #3, forward	ACTGCTCCTTCTGCCTGACC
H8270	*TRAF2* RT-qPCR for siRNA #3, reverse	TTCTTTCAAGGTCCCCTTCC
H8271	*GAPDH* RT-qPCR, forward	TCGTCCCGTAGACAAAATGG
H8272	*GAPDH* RT-qPCR, reverse	CTCCTGGAAGATGGTGATGG
H8322	*MYL1* 3f RT-qPCR, forward	TGCTGACCAGATTGCCGACTTCA
H8323	*MYL1* 3f RT-qPCR, reverse	CCCGGAGGACGTCTCCCACC
H8326	*AHCY* RT-qPCR, forward	GGTGCTGAGGTGCGGTGGTC
H8327	*AHCY* RT-qPCR, reverse	GGGTCCGTCCTTGAAGTGCAGC
H8328	*TNNC1* RT-qPCR, forward	GCACCAAGGAGCTGGGCAAGG
H8329	*TNNC1* RT-qPCR, reverse	TGTGCCACTGCCATCCTCGT
H9054	*cIAP1* (*BIRC2*) RT-qPCR, forward	TAGTGTTCCTGTTCAGCCCG
H9055	*cIAP1* (*BIRC2*) RT-qPCR, reverse	TCCCAACATCTCAAGCCACC
H9056	*cIAP2* (*BIRC3*) RT-qPCR, forward	ACGATTTAAAGGTATCGCGCC
H9057	*cIAP2* (*BIRC3*) RT-qPCR, reverse	CTGATACCGCAGCCCACTTC
H9076	*XIAP* (*BIRC4*) RT-qPCR, forward	ACGGAGGATGAGTCAAGTCAAA
H9077	*XIAP* (*BIRC4*) RT-qPCR, reverse	AAGTGACCAGATGTCCACAAGG
H9080	*BRUCE* (*BIRC6*) RT-qPCR, forward	CCAGTGTGAGGAGTGGATTGC
H9081	*BRUCE* (*BIRC6*) RT-qPCR, reverse	CCTCAATGTCCGGATCTAAGCC